Coastal Engineering 87 (2014) 50–76

Contents lists available at ScienceDirect

Coastal Engineering

journal homepage: www.elsevier.com/locate/coastaleng

An approach to assess flooding and erosion risk for open beaches in a changing climate

M. Villatoro [a,*], R. Silva [a,*], F.J. Méndez [b], B. Zanuttigh [c], S. Pan [d,1], E. Trifonova [e], I.J. Losada [b], C. Izaguirre [b], D. Simmonds [d], D.E. Reeve [d,2], E. Mendoza [a], L. Martinelli [f,g], S.M. Formentin [c], P. Galiatsatou [h], P. Eftimova [e]

[a] Instituto de Ingeniería, Universidad Nacional Autónoma de México, Cd. Universitaria, 04510 D.F., Mexico
[b] Environmental Hydraulics Institute "IH Cantabria", Universidad de Cantabria, Spain
[c] University of Bologna, DICAM, Viale Risorgimento 2, 40136 Bologna, Italy
[d] University of Plymouth, Drake Circus, Plymouth PL4 8AA, UK
[e] Institute of Oceanology, Bulgarian Academy of Sciences, Parvi Mai Str. 40, P.O. Box 152, 9000 Varna, Bulgaria
[f] ICEA, University of Padova, Via Ognissanti 39, 35129 Padova, Italy
[g] CORILA, Italy
[h] Aristotle University of Thessaloniki, Hydraulics Laboratory, 54124 Thessaloniki, Greece

ARTICLE INFO

Article history:
Received 12 June 2013
Received in revised form 20 November 2013
Accepted 22 November 2013
Available online 2 January 2014

Keywords:
Coastal risk
Flooding
Erosion
Sources
Hazard
Extreme event
SPRC

ABSTRACT

This paper examines the vulnerability to flooding and erosion of four open beach study sites in Europe. A framework for the quantitative estimation of present and future coastal flood and erosion risks is established using methods, data and tools from across a range of disciplines, including topographic and bathymetric data, climate data from observation, hindcast and model projections, statistical modelling of current and future climates and integrated risk analysis tools. Uncertainties in the estimation of future coastal system dynamics are considered, as are the consequences for the inland systems. Different implementations of the framework are applied to the study sites which have different wave, tidal and surge climate conditions. These sites are: Santander, Spain—the Atlantic Ocean; Bellocchio, Italy—the Adriatic Sea; Varna, Bulgaria—the Black Sea; and the Teign Estuary, UK—the northern Atlantic Ocean. The complexity of each system is first simplified by sub-division into coastal "impact units" defined by homogeneity in the local key forcing parameters: wave, wind, tide, river discharge, run-off, etc. This reduces the simulation to that of a number of simpler linear problems which are treated by applying the first two components of the Source–Pathway–Receptor–Consequence (S–P–R–C) approach. The case studies reveal the flexibility of this approach, which is found useful for the rapid assessment of the risks of flooding and erosion for a range of scenarios and the likely effectiveness of flood defences.

1. Introduction

The European coastline is one of the most densely populated and developed coasts in the world. Up to half the population of Europe's coastal states now lives within 50 km from the coastline (Eurostat, 2009), attracted to this dynamic hinterland for transportation, commercial or recreational purposes. Many of these coastal communities are vulnerable to erosion and flooding events, putting a great number of people and valuable infrastructure at risk. Similarly, coastal habitats — sandy beaches, coastal lagoons and sedimentary cliffs, etc. are also threatened, a matter made worst by coastal squeeze from these communities. This makes it vital that the imminent arrival of coastal threats should be predicted in order to enable communities and civil protection agencies to respond in a timely fashion, and for hazard-reduction measures to be in place.

However, the assessment of flooding and erosion risk on the coast is a complex problem, due to the large spatial variability of marine dynamics, geological, ecological and urban coastal environments, defence and protection measures, etc. Until the end of the twentieth century, traditional methods of estimating the sources of flood and erosion risk were dominated by the statistical analysis of historical data (Thorne et al., 2007). However, due to the short time scales covered by the majority of the available records, this often meant ignoring longer term trends, such as those resulting from climate variability and human induced sea level rise. The arrival of important advances in hydrodynamic modelling and GIS techniques, as well as a deeper understanding of the nature and impacts of climate change during the last 30 years, has allowed these complexities and limitations to be dealt with more efficiently. Climate change, with its associated rising sea level and possible increases in the frequency and/or intensity of storms and changes in wave climate, can be expected to significantly increase the risk of coastal erosion and flooding in most coastal locations (Nicholls

* Corresponding authors. Tel.: +52 55 5623 3600x8633, 3668.
E-mail addresses: MVillatoroL@iingen.unam.mx (M. Villatoro), RSilvaC@iingen.unam.mx (R. Silva).
[1] Currently, School of Engineering, Cardiff University, Cardiff CF24 3AA, UK.
[2] Currently, College of Engineering, Swansea University, Swansea SA2 8PP, UK.

0378-3839/$ – see front matter © 2013 Elsevier B.V. All rights reserved.
http://dx.doi.org/10.1016/j.coastaleng.2013.11.009

et al., 2007). On the other hand, developments in hindcasting and climate modelling have resulted in improvements to coastal storm predictions such that the timing, intensity and other important storm variables can be forecast quite accurately up to approximately three days in advance. Finally, the improved ability to precisely model the extent of flooding or erosion over large geographical areas has been of great use in risk management.

In this paper, the most recent advances in hydrodynamic and morphological modelling are applied in order to identify the sources of risk of coastal flooding and erosion (hazards) and their interaction with existing coastal defences (pathways) at four study sites across the Europe. Despite the different models and techniques used at each study site, a consistent analysis framework, provided by the **SPRC** approach, has been followed. This system evaluates how the **S**ources (waves, tide, storm surge, mean sea level, river discharge, run-off), through the **P**athways (coastal defence units), affect the **R**eceptor (inland system) generating **C**onsequences or damages (economical, social, environmental, affected population, land losses) (see Zanuttigh, 2011; Narayan et al., in this issue). The first step is the identification of the main features to be analysed (beaches, coastal defences, inland areas) at each site and the most relevant marine and river dynamics (waves, sea level, tide, storm surge, river discharge, run-off) that define the Sources. Within the region of interest a number of sources, N_s, are identified. These are chosen to sufficiently characterise the major sources of hydrodynamic forcing within the system. A source may comprise a wave climate (wave height, wave period, wave direction) or other sets of variables describing tides, surges, river discharges or mean sea levels. Then, the coastline is divided into N_p homogeneous "pathway" units. This segments and classifies the entire shoreline into a limited number of coherent typologies, encompassing man-made and geomorphological features. Finally, the hinterland is divided into N_i "receptors" or impact units, which are regions with similar properties and susceptible to similar threats, perhaps dictated by elevation, land use or ecology or geomorphology. After establishing the impact units, we need to define the different hazards that affect them through the pathways and characterise their statistical distribution.

The approach is exemplified in a practical fashion through the application of key parts of the proposed analysis framework to four different study sites, located in Italy, Bulgaria, Spain and the UK. The Italian case study at Bellocchio is focused mainly on the application of a high resolution flooding model and the advantages of using LiDAR as input for such models. It also analyses the role of existing flood and erosion management in the degree of exposure and presents a comparison of the results of flooding considering a) different time slices (current and future epochs) and b) failure scenarios. The second study site, Varna in Bulgaria, provides detailed coverage of storm surge modelling and the selection of scenarios which are represented as *Intensity–Duration–Frequency* (IDF) plots. It presents a comparison of the application of 3 morphodynamic models and qualitative flooding and erosion maps for a variety of scenarios. The Spanish contribution places more attention on the definition of sources and hazards and their statistical characterisation, applied to a specific local scale area, i.e. Santander in northern Spain. They focus on the first steps of the methodology, downscaling the sources into the area around Santander while defining and characterising flooding and erosion hazard pdfs ($f(z)$). Finally, the study site from South Devon in the UK applies statistical analysis to existing hydrodynamic data in order to generate erosion and flood maps, for present and future scenarios, through GIS technologies.

2. Italian case study: Present and future flooding in Bellocchio

2.1. Site description

The Po River delta and the adjoining coast, which developed out of the Adriatic Sea, are surrounded by the Venice lagoon in the north and the sandy coastal zone of the Romagna (Ravenna) with the Po plain to the rear, at the South up to the promontory of Gabicce, where the Apennines Mountains meet the Adriatic Sea. It covers an area of 73,000 ha, of which 60,000 is reclaimed land and the remainder are brackish lagoons, with dams or open foreshores and emerging sandy banks.

The impact of this site for the Italian economy can be summarised with a few figures, valid for 2006, relative to tourism activities: 41 M person/days in the period May–September; 3384 hotels; 154,000 employees; and a gross income per year of €9.8 billion.

A general erosive tendency is mainly caused by a reduction in sediment supply from the rivers and by the increased anthropogenic subsidence. Subsidence, eustatism and erosion of dunes pose a serious threat for coastal flooding. Most intense storm events come from Bora (NE) and Scirocco (SE); with the one year wave height being 3.5 m and the 1 in 100 year wave height being 6 m. The wind is stronger and colder from the shorter fetch sector of Bora where it frequently reaches 35 knots, whereas from the long fetch sector of Scirocco it seldom exceeds 30 knots and is typically warm. The tidal excursion is low; the average spring tide range is ± 0.4 m and extreme year values are around $\pm$ 0.85 m.

The site of Bellocchio extends from the outflow of the Reno River in the South, to the Porto Garibaldi canal harbour in the north (Fig. 1). It includes highly urbanised touristic resorts, famous for the wide and sandy beaches (Lido degli Estensi and Lido di Spina), as well as natural areas of the Po Delta Park (Vene di Bellocchio), famous for bird-watching and other wildlife resources. The landward boundary of the site follows the route of the Romea road and the eastern limit of the Comacchio Valleys, which are particularly important for fishing and aquaculture activities.

The site can be ideally divided into three morphological areas (Fig. 2):

- the southern area, from the Reno River mouth to the Gobbino channel; approximately 2 km long, this area is still accumulating some material. Although the coastline is stable, the seabed gained 260,000 m^3 of sediment from 2000 to 2006. Sediments come from the erosion of the sandy spit, since the Reno river does not provide a considerable amount of sediment at present (due to construction of docks);
- the central area, from the Gobbino channel to the tourist resort of Lido di Spina; the greatest erosion rate of the whole Adriatic littoral was registered along this stretch (approximately 11 m/year); around 750,000 m^2 of sediment and 200 m of beach were lost between 1982 and 2006. The shoreline retreat is now threatening adjacent low-lying areas, with great naturalistic and environmental value. Erosion and breaching of reconstructed dunes have also occurred, shifting their position further back.
- the northern area, from Lido di Spina to Porto Garibaldi; it is characterised by deposition of sediments transported northwards from the Reno outflow and intercepted by the jetty of Porto Garibaldi, increasing the local beach width (up to 300 m). It is estimated that 4.1 Mm^3 has accumulated in this area from the shoreline to the closure depth.

The whole area has suffered from anthropogenic subsidence since the 1970s. Between 1999 and 2005, the subsidence rate was in the range of 4–7.5 mm/year, in addition to the natural land lowering of 0.3 mm/year. Maximum subsidence values occur at Porto Garibaldi, where a total land lowering of 0.18 m has been recorded (Preti et al., 2009).

Existing flooding and erosion management strategies at the study site can be divided into three groups: beach re-nourishment activities, using sand accumulated at Lido degli Estensi to nourish adjacent beaches; construction of defences, such as dikes, groynes and stone revetments; and drainage/irrigation systems, which consist of channels, valves and pumping stations that drain water out from the floodable area and into the sea. At present, there are two main issues that are considered by coastal managers for the safety of this coastal area: the

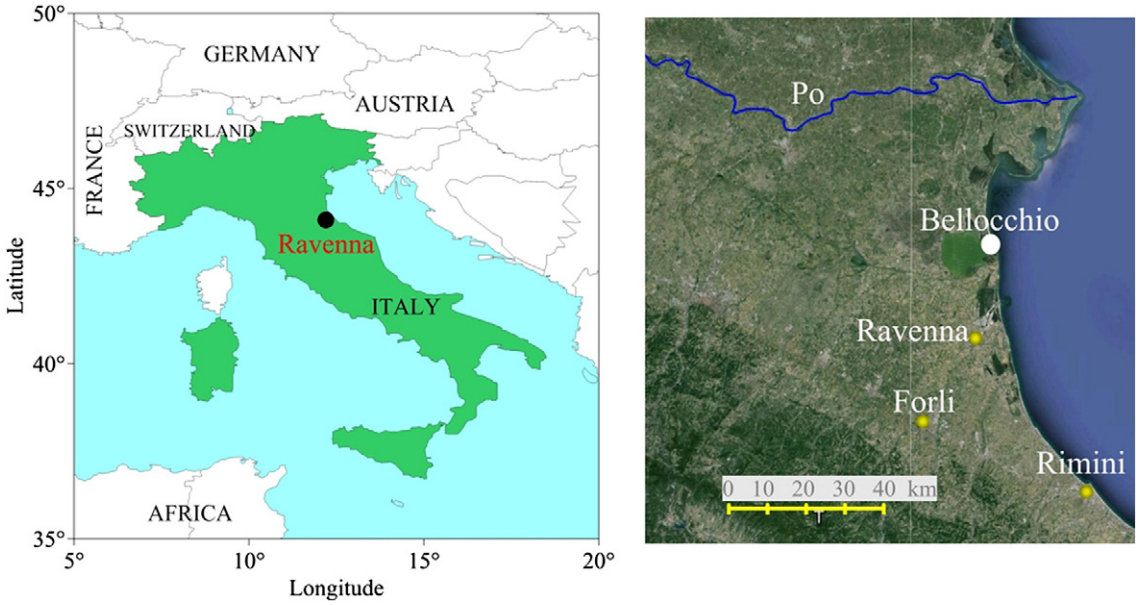

Fig. 1. Location of the site of Bellocchio in the Emilia Romagna region, Adriatic Sea, Italy.

eventual breaching of the sea bank between the Ancona di Bellocchio and the Spina lake, and; the elevation of the banks (now +1.4 m MSL) of the marina and the canal harbour of Porto Garibaldi.

Fig. 3 presents a large-scale SPRC scheme relative to Bellocchio, with the purpose of identifying the main conceptual units within the site. It shows the main sources, i.e. river flooding, water level in the channels, and the combination waves, tide and surge at the shoreline. Drivers such as subsidence are implicit in the scheme. The main pathways (which may also be considered as receptors of lower intrinsic value), the receptors (that may also be pathways for other receptors), and the major possible consequences in the different sites are also shown.

The small-scale analysis evaluates the actual proximity of the receptor to the source and is studied with a detailed small-scale analysis performed at pixel level, based on altimetric LiDAR surveys and land use maps.

LiDAR data available for this area has very fine resolution (1 m), allowing a detailed analysis of its features, and thus the identification of the most critical pathways for coastal flooding. This is particularly useful in low lying areas, such as in Bellocchio, and when one wishes to model flooding in urban areas with narrow streets where a very detailed mesh is needed.

2.2. Data

2.2.1. Climate conditions

The meteorological data were derived from the regional downscaling of the SGA-CLM (COSMO-CLM) data sets. A control period (1960–1990) and the three periods of the IPCC A1B scenario (2010–2039, 2040–2069, 2070–2100) were considered. Details about the methodology can be found in Umgiesser et al. (2011) and Weisse et al. (2014–in this issue).

The yearly maximum wave and storm surge conditions for the period 1960–1990, characterised by significant wave height, peak off-shore wave steepness, wave direction and water elevation (sum of storm surge and tide), were processed to derive the climate statistics describing the yearly probability of occurrence of each storm at present. The joint statistics obtained by assuming respectively the wave height H_s or the surge level η_s as first variable are reported in Table 1. The data for other time slices were elaborated in a similar way. The synthesis of the extreme climate conditions at present and in the short, medium and long term scenarios are reported in Table 2. The analysis of the storm development showed that the typical duration of the storm peak is 12 h, the rise-time from $H_s = 0.5$ to 3.5 m is of the order of 12 h, while the minimum fall-time from $H_s = 3.5$ to 0.5 m is 28 h.

2.2.2. Topo-bathymetric surveys

Available topographic data in the area include periodic cross-shore single-beam bathymetric surveys and topo-bathymetric LiDAR surveys. In regard to the high resolution of the LiDAR, specific attention has to be paid to the interpretation of the acquired data for modelling purposes. For instance an element like a tree should be distinguished from a building by means of appropriate pre-processing and then represented as a local increase of roughness rather than included in the bathymetry as a local change of the bottom elevation.

2.3. Methodology: Flood modelling

2.3.1. A procedure for the representation of wave run-up and transmission

In order to define in a simple and quantitative way the flooding process, the proposed failure mechanism is the sea ingression by overtopping of a dune, a beach, a road, or any other physical barrier placed along the coastline. The overtopping mechanism is described by

$$(\eta_s + S_r + h + R_{u2\%}) - R_{c0} \geq 0 \quad (1)$$

where η_s is the storm surge level, S_r is the sea level rise induced by climate change effects; η_ω is thewave set-up; $R_{u2\%}$ is the wave run-up corresponding to the characteristic value of 2% exceeding probability; and R_{c0} is the crest height of the sea bank (equal to the beach height plus the dune height, if applicable). Eq. (1) is based on the following simplified assumptions: non erodible beach profile; absence of defence breaching against wave and tidal loads, and; missing representation of subsidence.

Further, the failure function does not account for the magnitude of inland flooding (e.g., the effect of few overtopping waves is not distinguished from the effect of a complete flood), thus overestimating the damage consequences. In practice, since the limit state causing failure in Eq. (1) is represented by $R_{u2\%}$, it can be considered that failure is caused by some degree of flooding which is perceived by the local inhabitants.

Waves are transformed for a given tidal range from offshore to the shore, including wave reduction due to structures where applicable, by means of an analytical Matlab® procedure. Wave transmission across detached barriers, if present, is accounted for by means of simple

Fig. 2. Left, aerial view of the site. Right, from top to bottom, views of Lido degli Estensi with Porto Garibaldi canal harbour and the marina; erosion close to the Ancona di Bellocchio area; Vene di Bellocchio; vegetated sand and soil dike protecting the Valleys close to Gobbino.

formulae (van der Meer et al., 2005), whereas it is assumed that no wave reduction occurs across gaps. Total transmission in the protected area is then obtained by balancing energies. Hence, wave run-up is computed by means of the equation proposed by Stockdon et al. (2006):

$$R_{u2\%} = 1.1\left\{0.35\tan\beta(H_s L_0)^{1/2} + 0.5\left[H_0 L_0\left(0.563\tan\beta^2 + 0.004\right)\right]^{1/2}\right\} \quad (2)$$

where H_s is the off-shore significant wave height and L_0 is the off-shore peak wave length, β is the beach slope defined as the average slope over a region of two times the standard deviation of a continuous water-level record (β is about 0.01). The formula already accounts for wave set-up η_ω on natural beaches.

2.3.2. Modelling with MIKE21

The flood simulation was performed with MIKE21 HD FM (DHI, 2007), using data from the LiDAR surveys as input for the bathymetry (see Fig. 4).

Waves are transferred for a given tidal range from offshore to the shore by means of the same procedure described in the previous Section 2.3.1. Then, a random phase Gaussian process is generated having a 2% characteristic value consistent with the value of $R_{u2\%}$ estimated from Eq. (2). The "off-shore" boundary is thus moved to the shoreline

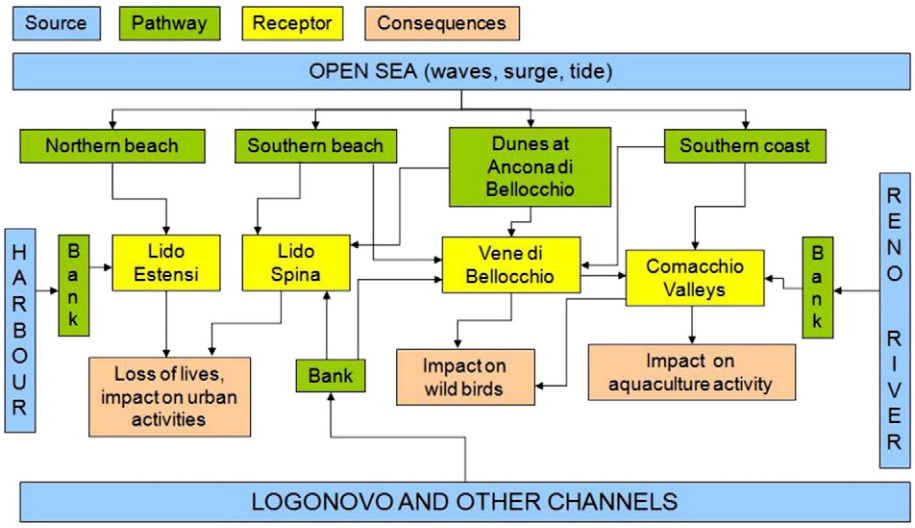

Fig. 3. SPRC analysis for Bellocchio.

and the "shoreline" boundary condition considers a varying level in time $W(t)$ that is actually given by the sum of storm surge, wave set-up and wave run-up on the beach —both included in Eq. (2).

The flooding wave propagation is then simulated as a dam-break at the shoreline. The "dam-break" solution is preferred to a flux condition since there is no formula available in the literature for representing discharge at sea banks (but only discharge at emerged structures/dykes). Wave celerity is thus indirectly represented by adding wave run-up (potential wave energy at the shoreline) as a component of the water level $W(t)$ imposed at the shoreline. The wave propagation methodology is described in detail in Martinelli et al. (2010).

Lateral and inland boundaries are set to be land boundaries. The computational domain is enlarged to avoid spurious reflection effects. To improve accuracy of the results, the part of the shoreline boundary which is closest to the lateral boundaries is also set as land boundaries (around 500 m long-shore to the north and to the south of the domain). At the inland boundary the river/channel discharges are given along the river/channel section (average annual conditions). The conditions at the river/channel outflows are unknown. A preliminary MIKE21 Coupled FM simulation on a coarse grid is therefore required to assess water levels at the outlet in time. Based on the results obtained from the simulations for the present scenarios, it can be assumed that at the channel and river outlet the storm surge level is reached within a time compatible with the history level imposed at the shoreline boundary.

Table 1
Fitting of: A) yearly incident significant wave height (H_s), and conditioned values of offshore peak wave steepness (s_{op}), wave direction (Dir) and storm surge level η_s (including tide); B) yearly incident significant storm surge level η_s, and conditioned values of H_s, s_{op}, Dir.

A	H_s (m)	s_{op}	Dir (°)	η_s (m)
Type	Weibull	Normal	Normal	Normal
Dir < 90°N				
Mean	4.140	0.045	83	$-0.3 + 0.25^{*}H_s$
Std	0.760	0.005	10	0,193
Dir > 90°N				
Mean	3.800	0.041	113	$0.32 + 0.19^{*}H_s$
Standard deviation	0.596	0.004	5	0.129
B	η_s (m)	H_s (m)	s_{op}	Dir (°)
Type	Normal	Normal	Normal	Normal
Dir > 90°N				
Mean	1.255	2.781	0.028	118
Standard deviation	0.124	0.766	0.009	11

Due to the high complexity of the areas and to the required limitation of the computational effort the following steps are considered for the flood simulation: buildings were excluded from the computational domain; the triangle cell sizes variation from 3 m to 50 m were used depending on the areas of interest; variable Manning coefficient based on the corresponding land use map available from the Regional Authority: 30 $m^{1/3}/s$ for emerged beach, 40 $m^{1/3}/s$ for urban area and streets, 30 $m^{1/3}/s$ for river banks and vegetated river sections, 20 $m^{1/3}/s$ for grass, fields, woods; Smagorinsky formulation for eddy viscosity, with constant eddy coefficient, and; constant discharges (typical average discharges) at the river/channel inlets.

2.4. Results

The flood simulations considered are: three climate scenarios (short 2020s, mid 2050s and long 2080s term) for sea level rise, storm and surge (see Table 2); two storm surges combined with wave conditions reproducing a frequent and a severe storm, characterised by 10 and 50 years return periods respectively (see Table 2); typical storm duration of 12 h (peak storm conditions) plus 2 h of rising phase and 2 h of descending phase; present (2010) estimates of average annual river and channel discharges based on historical data; no subsidence, and; the most probable failure of existing defences, based on the analysis of the system and on stakeholders opinion: the formation of a breach in the sea bank (see Fig. 5). The sea bank already shows, at present, a

Table 2
Extreme conditions (surge is the first variable of the joint statistics) in Bellocchio. Storm surge level η_s, associated to significant wave height H_s, seal level rise S_r. Wave direction >90°N.

Scenario	S_r (m)		Return period (years)							
			2	5	10	20	25	30	50	100
2010	0	S_{op} (%)	1.53	2.27	2.65	2.97	3.06	3.13	3.33	3.56
Present		η_s (m)	1.26	1.37	1.43	1.48	1.49	1.50	1.53	1.57
		H_s (m)	2.78	3.67	4.13	4.51	4.62	4.71	4.93	5.20
2020	0.07	S_{op} (%)	1.49	2.02	2.30	2.53	2.60	2.65	2.79	2.96
Short term		η_s (m)	1.22	1.32	1.37	1.41	1.42	1.43	1.45	1.48
		H_s (m)	2.80	3.51	3.86	4.14	4.22	4.28	4.44	4.64
2050	0.13	S_{op} (%)	1.59	2.16	2.41	2.77	2.98	2.90	2.99	3.12
Mid term		η_s (m)	1.24	1.35	1.40	1.45	1.46	1.47	1.50	1.53
		H_s (m)	2.78	3.56	3.90	4.20	4.26	4.39	4.51	4.82
2080	0.22	S_{op} (%)	1.55	2.26	2.64	2.95	3.04	3.11	3.30	3.53
Long term		η_s (m)	1.28	1.42	1.50	1.56	1.58	1.59	1.63	1.67
		H_s (m)	2.72	3.56	3.99	4.34	4.44	4.52	4.73	4.98

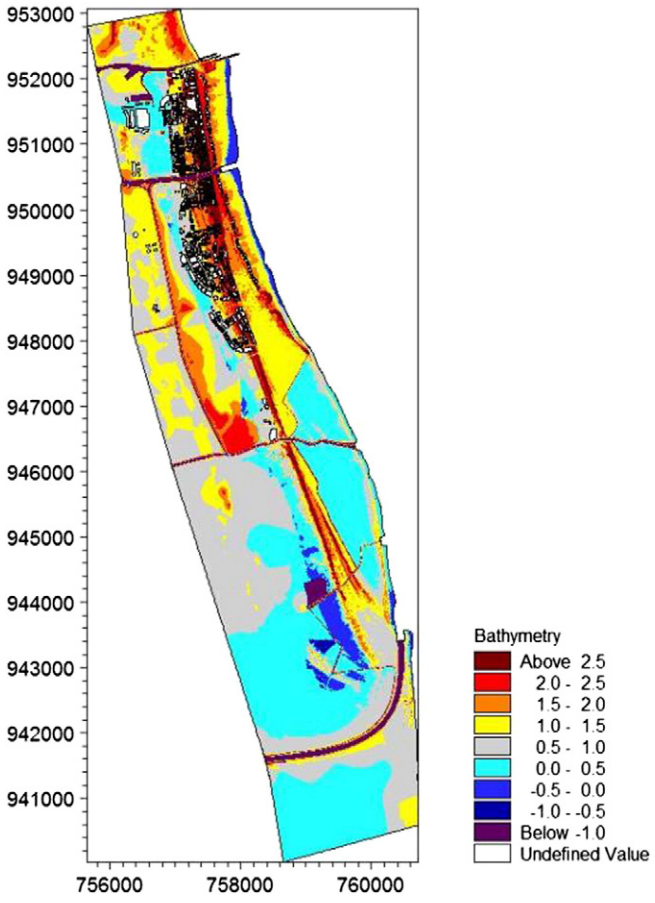

Fig. 4. Bathymetry map; colours from grey to violet indicate surface elevation ≤1.0 m MSL.

breach, 20 m long, seen in the bottom elevation map. The breach does not evolve in time during the simulation.

Figs. 6 and 7 show the maps of maximum surface elevations and maximum velocities derived from MIKE21, accounting for sea level rise and river discharges but disregarding subsidence, and in case of breaching.

The following three areas are flooded in all simulated conditions immediately after the start of the storm, with quite large depths (surface elevation > 2.2 m) and velocities (>1 m/s):

- the Ancona di Bellocchio. The frequent and intense flooding of the Ancona di Bellocchio suggests that this area of high ecological value inside the Po Delta Park may be irreversibly damaged. According to simulations, flooding occurs in all conditions, i.e. also for a 2 year return period, which is also in agreement with observations. It should be clarified whether the strategy is to defend or to leave this area to be submerged, also in view of further reinforcement of the sea banks. Even in the long term scenarios, water does not propagate further inland thanks to the existing banks so that maintenance of these may be sufficient;
- the beaches of Lido degli Estensi and of Lido di Spina. The values of flooding depths and velocities suggest that beach reshaping may play a relevant role in the eventual flood of the urban area behind the bathing facilities; the maintenance of beach width therefore plays an essential role in the defence of the urban area;
- the area close to the Reno river outlet. In the long term scenarios the river–sea interaction is evident, with overflow occurring along the northern river bank. In the short term scenarios (and present), the military area to the south of the outlet, already suffering from great erosion, is exposed to flood.

Both urban areas of Lido degli Estensi and Lido di Spina are naturally protected due to the construction of this area on the ancient dunes (i.e. higher bottom elevation). The inland parts of these areas are both flooded in case of long term (2080) scenarios; Lido degli Estensi is flooded actually also in the mid-term (2050) in presence of intense storms ($T_r \geq 50$ years).

Providing that beaches and sea banks are maintained, the flooding of the urban areas is generated by the overflow from the canal harbour and from the marina (right hand-side). Adequate attention is therefore required to the channel regulation and to the banks. The canal harbour and the marina banks are under-designed: only in the short term scenario (2020) and without accounting for subsidence they do not show any overflow. It is therefore suggested to make the sea banks higher, at least up to 2.5 m MSL Lido degli Estensi results much more exposed at risk than Lido di Spina.

Overflow at the sea bank between the Ancona di Bellocchio and the Lake of Spina occurs even in case the breach is not artificially made in the DTM. Effects are obviously less marked in this case. When the breach in the sea bank occurs, the water overflows the sea bank, fills the lake and propagates towards the urban area of Lido di Spina. The area closer to the beach in the southern part of Lido di Spina is reached by the flood, but the elevation of the urban area – together maybe with the limited duration of the simulated storm event – provides safe conditions for inhabitants. Rural areas are flooded in long term (2080) scenarios by the overflowing of the channel banks due to sea–river interaction.

It is worth noting that the modelling methodology does not take into account beach reshaping during the storm. The beach of Lido degli Estensi is particularly wide, becoming totally submerged during the storm; the beach of Lido di Spina is narrower, almost disappearing in the southern part close to the wooden groynes. It is therefore imperative to couple the monitoring and maintenance plan of the sea bank with appropriate beach maintenance.

3. Bulgarian case study: Extreme flooding and erosion in varna

3.1. Site description

The Varna study site is located in the Western Black Sea, between capes Ekrene and Galata (Fig. 8). It covers four beaches in the Western Black Sea region — Golden sands, Kabakum, Varna Central and Karantinata, all of which are subject to frequent flooding and chronic erosion.

The Bulgarian Black Sea coast has eastern exposure and storms which typically approach from the NE, E and SE can cause serious damage to coastal regions (Valchev et al., 2007). Historical records of extreme hydro-climatic events show that for the Western Black Sea shelf storm waves and sea level fluctuations are the most dangerous sources of flood hazard (Andreeva et al., 2011; Belberov et al., 1982; Stakev, 1980; Trifonova et al., 2011).

Fig. 9 presents a large-scale SPRC scheme relative to Varna, with the purpose of identifying the main conceptual units within the site. The location of the Black sea and its restricted connection to the oceans define it as a non-tidal basin with tidal magnitudes ranging from 3 to 5 cm. The main sources of coastal flood and erosion in the Black sea are extreme rainfall (river floods) and storms (waves and storm surge). In spite of the fact that river input is very important for the water balance of the whole Black Sea basin and it defines seasonal sea level fluctuations, which for the Bulgarian coast are about 15 cm (Trifonova and Demireva, 2003), there are no major rivers in the close vicinity of the Varna study site. Consequently, for present climate conditions, only sea storms are considered as a source of flood and erosion risk at this particular study site. Extreme sea level rise and flooding of this coastal area are thus mostly due to the combination of storm surge and wave run-up.

From the perspective of predicted climate change scenarios, sea level rise is also a major potential hazard for the Varna coast. However, storm

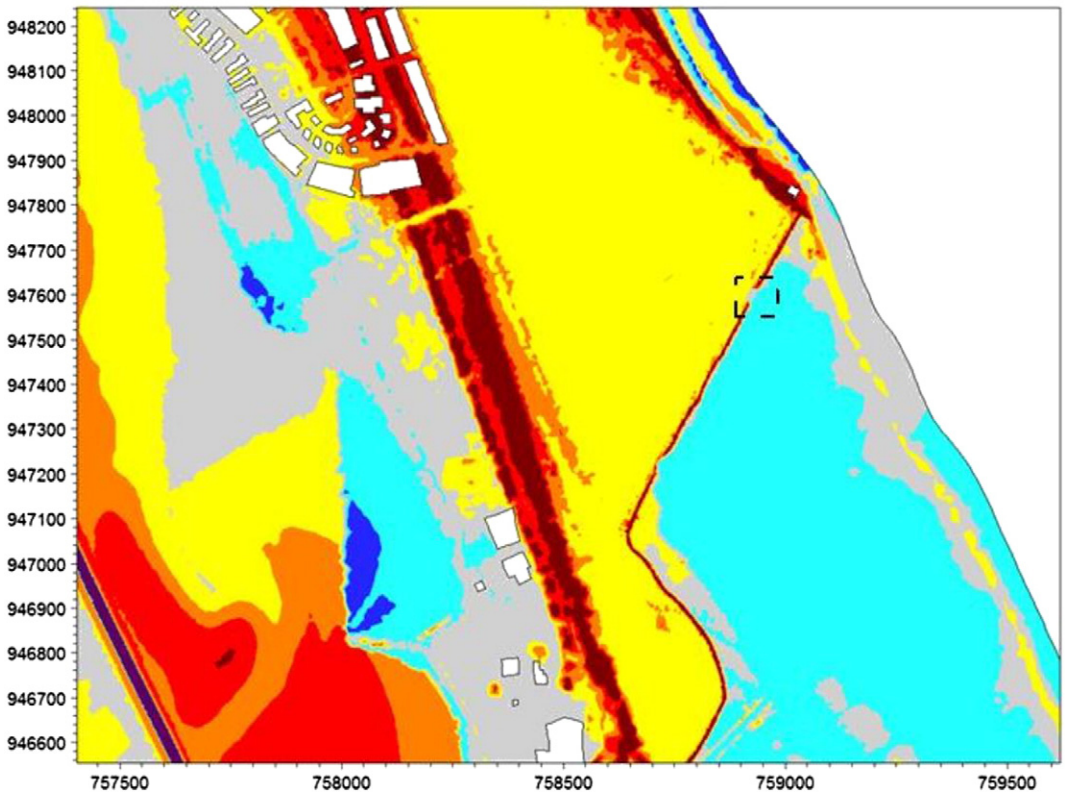

Fig. 5. Zoomed bathymetry close to the area where the breach is made (inside the dashed square).

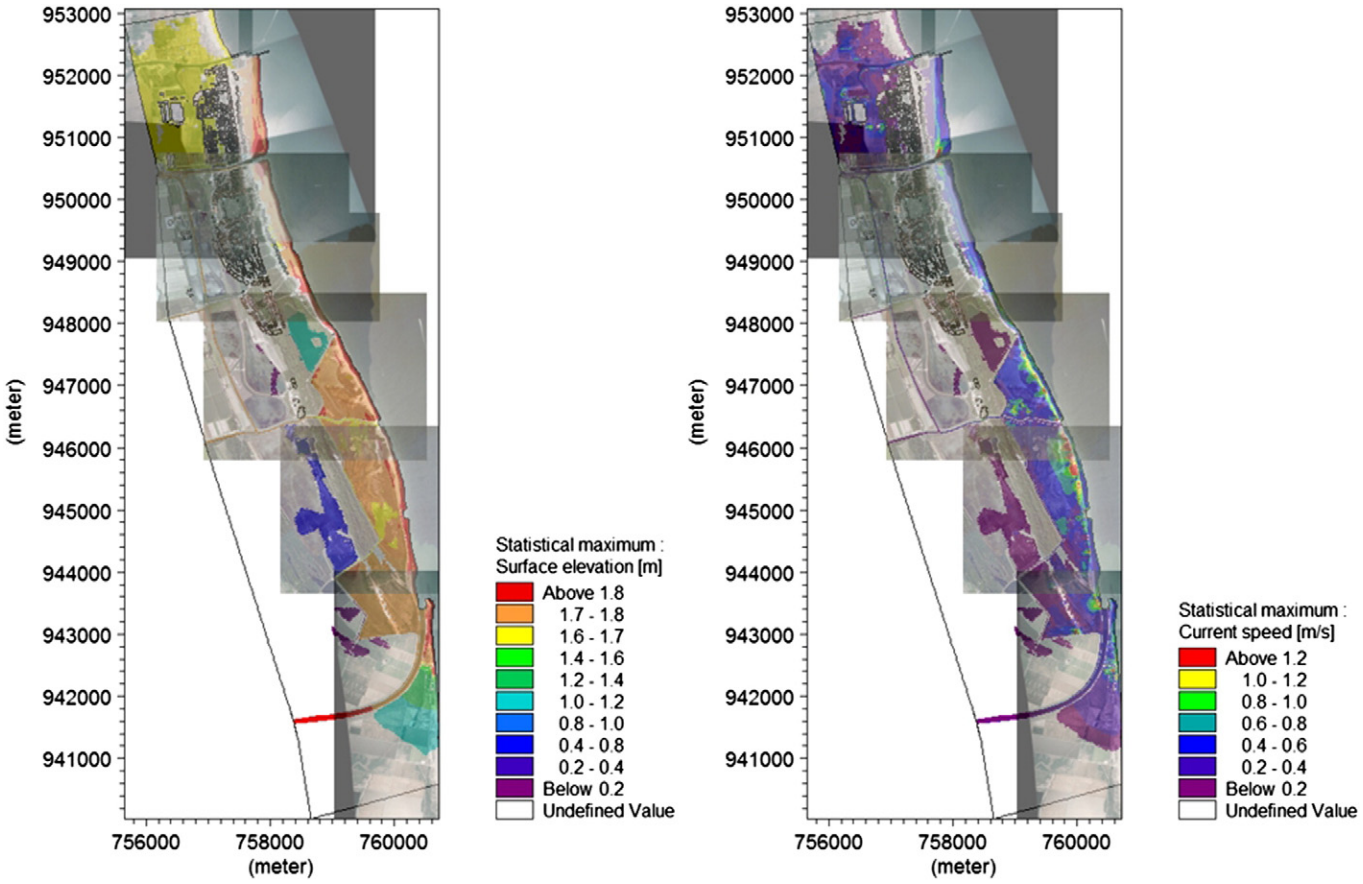

Fig. 6. Maximum flood depths (to the left) and velocities (to the right). Short term scenario (2020), $T_r = 100$ years. No breaching.

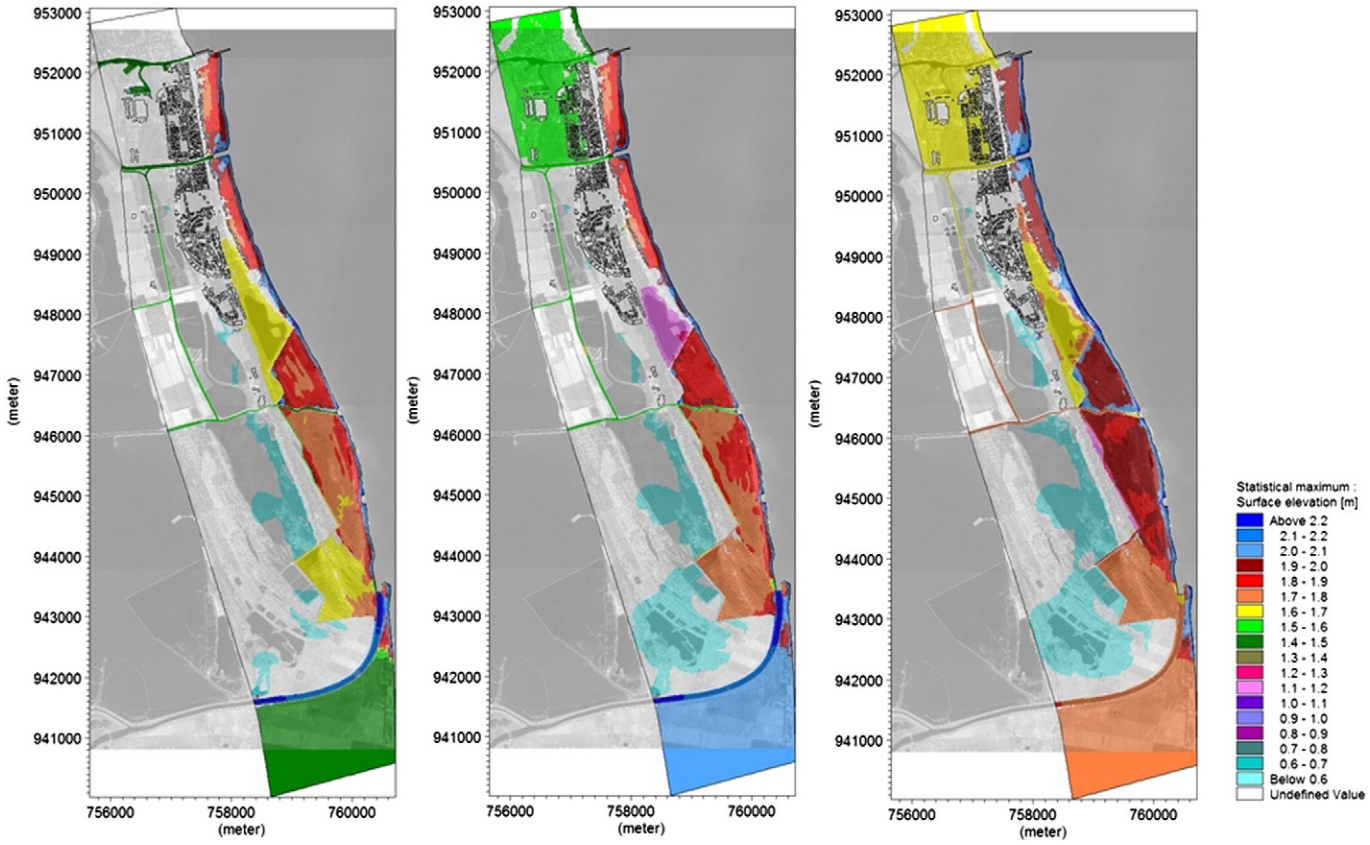

Fig. 7. Maximum flood depths (from left to right): short term scenario (2020) with breaching; mid (2050) and long term scenarios (2080) without breaching.

surge and sea level rise act at different time scales. For present climate conditions, deviation from the mean sea level caused by eastern storms (surge combined with wave run-up), for a return period 100 of years, is 3.23 m, while for future climate conditions, which include the gradual sea level rise due to climate change and changes in wave climate, an eastern storm with a return period of 100 years will cause a sea level deviation of 4.45 m. Therefore, for the present climate conditions the main sources of risk are those induced by storms, whereas for future climate conditions the impact of storm events on the coastal system is considered against a background of gradual sea level rise.

3.2. Data

In order to estimate the flood and erosion hazard in the Varna region, for both present and future climate conditions, various datasets were used, such as atmospheric reanalysis data, results of the CLM regional climate model, and detailed topography and bathymetry data.

Wind reanalysis data were used for the calculation of the wind forcing for the wave models. For present coastal dynamics the models WAM (Komen et al., 1994) and SWAN (Booij et al., 1999) were forced with global atmospheric pressure and wind reanalysis data from the

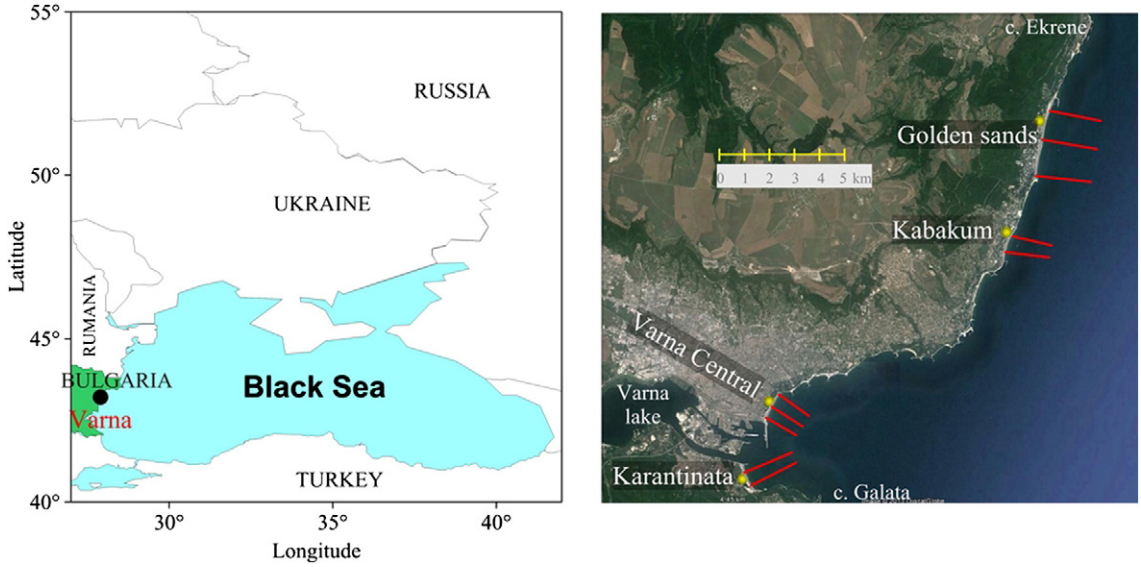

Fig. 8. Location of Varna coastal area, beaches subjected to flood, and selected cross-shore profiles.

European Centre for Medium-range Weather Forecast (Uppala et al., 2005), for a period of 61 years (1948–2008). For future coastal dynamics wave conditions were estimated using CLM regional climate model data for two IPCC scenarios: A1B and B1. Annual maxima of sea level data were extracted from time series of sea level available for Varna for the period 1928–2007.

To collect detailed topography and bathymetry for the implementation of the hydro- and morphodynamic models, an extensive field campaign was carried out in 2010. Based on the available data sets for nearshore bathymetry and the new bathymetry and topography, 10 typical cross-shore profiles were constructed. Three of them are at Golden sands beach, two at Kabakum beach, three at Varna beach and two at Karantinata beach. The location of the profiles is shown in Fig. 8.

3.3. Methodology: Scenario construction

It is assumed that maximum flooding and erosion result from extreme storm events. Flood and erosion conditions are estimated through numerical modelling. Two approaches have been implemented for the estimation of flood hazard. The first one is based on the maximum flood extent expected for a particular storm magnitude, while the other estimates the flood duration. Maximum erosion is determined by comparison of the initial and final (modelled) beach profiles.

Wave boundary conditions for both present and future climate scenarios were obtained by coupling the WAM wave model, adapted for fetch-limited conditions and run for the whole Black Sea basin, with the model SWAN, which is nested into WAM in order to propagate the waves in the western shelf zone (Valchev et al., 2007).

For the simulation of flooding and erosion, the prototype storm concept was employed to construct synthetic time series of wave height, period, direction and sea level during storms for specific return periods. Prototype storms for the present climate were constructed using wave reanalysis data, while for future climate CLM results for IPCC scenarios A1B and B1 were used. Firstly, the time series were subjected to a number of thresholds in order to identify individual storms (Trifonova et al., 2011; Valchev and Trifonova, 2009) and from these, a series of extreme events were selected (Valchev et al., 2012). The prototype storm has 3 phases – growth, full development and decay – by virtue of the fact that curves of significant wave height are described by a non-isosceles trapezium. The storm's growth stage is fixed to 30% of the total duration; the maximum development phase takes 20%; the decay is set to 50%. The prototype curve for surge level evolution is described by 5 phases, as the duration of maximum level is set to 4% of the total storm duration and coincides with maximum wave height.

Three storm directions (NE, E, and SE) are considered for four return periods (5, 20, 50, and 100 years) to form twelve storm prototypes for present climate conditions and twenty-four — for future climate. Key parameters considered for prototype shape construction are wave height, wave period, wave direction and sea level for storms with the considered return periods. Time series of annual maxima for both present and future climate conditions were processed using extreme value analysis and estimates of sea level deviations and wave parameters for certain return periods were obtained (Galiatsatou et al., 2012). Results of the analysis of extremes for different return periods are used as the peak values in the construction of prototype storms corresponding to the associated return periods.

A 2D hydrodynamic mathematical model (Krestenitis et al., 2010) was implemented in the Black Sea region for the prediction of the sea level rise (S_r) for future climate conditions taking into account atmospheric (wind, atmospheric pressure) and wave forcing (radiation stresses). Model results covering the period 2010–2100, for both climate scenarios A1B and B1, were produced. Table 3 presents the highest estimates of annual maximum wave height, corresponding wave period and annual maximum storm surge for three selected directions (NE, E, and SE).

Table 3
Estimates of annual maximum wave heights, wave periods and annual maximum storm surge.

Return period (years)	Present/ future	Eastern direction			North-eastern direction			South-eastern direction		
		H_s (m)	T (s)	η_s (m)	H_s (m)	T (s)	η_s (m)	H_s (m)	T (s)	η_s (m)
5	Present	5.22	6.86	0.28	3.79	5.31	0.26	3.92	6.05	0.29
20		5.62	7.47	0.4	4.48	5.8	0.32	4.9	6.8	0.39
50		5.74	7.84	0.53	4.83	6.01	0.37	5.38	7.21	0.5
100		5.82	8.13	0.62	5.01	6.12	0.43	5.79	7.53	0.58
5	A1B	3.96	6.4	0.7	2.48	4.45	0.7	2.95	5.3	0.7
20		4.88	7.28	0.88	2.97	4.89	0.88	3.75	6.21	0.87
50		5.47	7.84	0.99	3.28	5.16	0.99	4.26	6.7	0.98
100		5.9	8.25	1.08	3.51	5.37	1.08	4.64	7.07	1.05
5	B1	4.12	6.52	0.71	2.53	4.45	0.7	3.12	5.44	0.71
20		5.09	7.48	0.87	3.04	4.96	0.87	3.92	6.21	0.87
50		5.71	8.09	0.98	3.37	5.25	0.98	4.43	6.7	0.98
100		6.18	8.54	1.05	3.61	5.47	1.05	4.81	7.07	1.05

Erosion during extreme storm events for the present climate was calculated using three morphodynamic models — IO-BASMM (Trifonova, 2007), SBeach (Larson and Kraus, 1989), and XBeach (Roelvink et al., 2009), while for future climate conditions, IO-BASMM was employed.

Flood conditions for both present and future climates were calculated using IO-BASMM. Each of the models was run along 10 selected profiles (see Fig. 8), forced by 12 prototype storms for present and 24 prototype storms for future climate conditions. As a result, time series of beach flooding and beach erosion were obtained for each storm prototype and for each beach profile. Erosion maps were compiled for the four selected beaches and maximum erosion of beach scarp was presented for selected beach sectors. Flood maps showing maximum flood extents were also produced.

Although flood and erosion due to sea storms usually occur at the same time, their impact depends on different factors. The analysis of historical storms shows that the damage caused by erosion is greater when more sand is lost from the beach, while damage due to flooding tends to increase with exposure time, i.e. the damage extent depends on storm duration as much as on the size of the flooded area. Therefore, in this study flood risk is estimated in relation to the time-span during which a certain location at the sub-aerial beach profile would remain under water during a storm of a given return period. Thus, flood scenarios are presented as a relationship between the cross-shore beach elevation and the flood duration for this specific elevation. To consider the effects of sea level rise in the risk of flooding and erosion in the Varna coastal region, the changes in sea level due to climate change were accounted for short- (2020), mid- (2050) and long-term (2080) horizons. Sea level time series for each prototype storm were adjusted with respect to the prediction for mean sea level rise. As a result storm prototypes for short-tem, mid-term, and long-term horizons were modified and subsequently used as hydrodynamic boundary conditions for the hydrodynamic module of IO-BASMM. For each scenario flood predictions are presented as a relation between beach elevation and flood duration for this specific elevation — *Intensity–Duration–Frequency* (IDF) curves relating flooding extent (elevation) and duration for 4 return periods — 5, 20, 50, 100 years.

All numerical experiments for present and future conditions were done using synthetic time series of key storm parameters – "storm prototypes". The methodology was tested against a series of historical storms reported in the literature (Andreeva et al., 2011). Time series of storm parameters (wave height, period and direction) were extracted from reanalysis (Valchev et al., 2012), and storm surge levels were calculated from wind fields with the model MATO (Posada et al., 2008). Classification of storms is performed using the database of storms, taking into account the most probable combination of directions

and intensities. As a result, the following scenarios for coastal area flooding were modelled: wind velocities (25, 50, 75, 100, 125 and 150 km/h) and wind directions (NE, ENE, E, ESE, SE and SSE). A total number of 36 cases were compiled, and based on the numerical results, transfer functions of the maximum storm surge as a function of wind velocity and direction were built, Eq. (3),

$$\eta_s = \frac{\alpha V + \beta V^2}{1000} \tag{3}$$

$$\alpha = a + \frac{b\theta}{100} + \frac{c\theta^2}{10000} \tag{4}$$

$$\beta = d + \frac{e\theta}{100} + \frac{f\theta^2}{10000} \tag{5}$$

where η_s is the maximum storm surge, V is the wind velocity in Km/h, θ is the wind direction and α and β are parameters evaluated through Eqs. (4) and (5), respectively. The values of the parameters a, b, c, d, e and f depend on the locations, some examples are shown in Table 4. The location of points for which the transfer functions were built corresponds to the deepest part of the 10 profiles modelled (see Fig. 8).

Two historical storms (February 1979 and March 2010) that took place in the western Black Sea were reconstructed using reanalysis data. The storm of February, 1979 was the most severe storm of the past century, causing considerable damage along entire Bulgarian Black Sea coast (Andreeva et al., 2011; Belberov et al., 1982; Stakev, 1980; Trifonova et al., 2010). During this event, the sea level at the Varna tide gauge was not measured because the station was flooded and out of operation. The hydrometeorological parameters of both events are presented in Table 5.

Storm surge patterns for selected beaches were reconstructed using the MATO surge model. The beach flooding was modelled using IO-BASMM.

3.4. Results

Flood maps represent the width of the flooded section of the beach as a % of total beach width, for an event with a specific return period. For each studied beach stretch twelve flood maps were constructed for present climate conditions and 24 maps for future climate conditions. The flooding magnitude is ranked in a four-colour scale, described in the legend of the relevant figures. An example calculated for present and future climate conditions for Varna beach is presented in Fig. 10.

Flood extent due to eastern storms considerably outmatches that caused by NE prototype storms for all four beaches – Golden sands, Kabakum, Varna, and Karantinata – and for both present and future climate. It is known that in the open sea NE winds are more intensive than eastern ones (Valchev et al., 2012), but due to the coastal orography they contribute to the generation of long-shore drift to a greater extent than to the surge level. The analysis of the results reveals that for a return period, T_r, of 5 and 20 years the flood extent due to eastern storms prevails over that caused by SE events. For T_r of 50 years the beach flooding caused by E and SE storms is almost commensurate, while for T_r of 100 years the flood extent produced by SE prototype storms is much greater than that caused by storms from the East.

Table 5
Significant wave height, surge level deviation and wind speed at the stage of maximum storm development for historical storms of February 1979 and March 2010 (after Trifonova et al., 2010).

Event	Duration (days)	H_s (m)	η_s (m)	V (m/s)	Maximum stage $H_s > 3$ m duration
February 1979	7 (16–22.02.1979)	4.58	1.4[a]	24	2.5 days
March 2010	5 (8–12.03.2010)	4.20	0.7	20	1 day

[a] Measured at Irakli station 50 km southward of Varna.

The southern portion of Golden Sands is the beach which is most threatened by flooding for all storms. Maximum flood extent is expected for eastern storms. Differences in flood extent between northern and southern portions of Kabakum beach are negligible. Maximum flooding of Karantinata beach is expected in its southern portion during E storms (more than 90% of the beach width would be flooded, even for $T_r = 5$ year). In spite of the fact that the width of the northern part of Varna beach is less than 30 m, and the southern one exceeds 100 m, the latter will be flooded more than 80% for $T_r = 5$ year of the eastern storms.

Erosion maps represent the width of the eroded section of the beach in % of the total beach width, for events with a specific return period. For each studied beach 36 erosion maps were constructed for present climate conditions and 24 maps for future climate conditions. All models forced with present climate conditions show maximum erosion for prototype storms from the East. As expected, the erosion pattern follows the one for flooding, namely that for $T_r = 5$ and 20 years the erosion due to eastern storms prevails over that caused by SE events. For $T_r = 50$ years the beach erosion caused by E and SE storms is almost commensurate. Example erosion maps for Varna beach, calculated with tree models, are presented in Fig. 11.

Results from the IO-BASMM model show that the southern portion of Golden Sands beach is more threatened by erosion caused by all storms. Maximum erosion is expected for eastern storms with 100-year return period — 10 m, which is equal to 38% of the beach width. Differences in erosion between the northern and southern portions of Kabakum beach are negligible. Maximum erosion of 9 m (14% of beach width) is predicted for eastern storms with a 100-year return period. Maximum erosion of Varna beach is expected in its northern portion where during eastern storms it reaches 7 m, which is about 29% of the beach width. At Karantinata beach during eastern storms maximum erosion reaches 7 m in the northern portion of the beach, which is 20% of beach width.

The results from Xbeach indicate that the northern portions of Golden Sands beach are most threatened by erosion produced by all storms, while at Kabakum beach — maximum erosion for all storms is observed at the northern part of the beach. Maximum erosion was calculated for the northern part of Varna central beach and the southern part of Karantinata. The results from SBeach indicate the same tendency, but with a higher magnitude — up to 38% of beach width is eroded at Golden Sands, 30% at Kabakum and more than 40% at Varna central and Karantinata.

From the perspective of the average beach erosion, all models predict the greatest erosion at Varna beach due to eastern storms (Table 6). The magnitudes of the average beach erosion correspond to wave forcing for relevant storm prototypes (Table 3), however the particular values of the maximum erosion differ for different wave approaches, and different locations. IO-BASMM predicted maximum erosion at the northern part of the beach for the eastern storms only

Table 4
Parameters for Eqs. (4) and (5), for three different locations.

Location	a	b	c	d	e	f
Golden sands resort	1.618209999	5.085748732	−2.613089948	−1.5424701	2.7128251	−0.8263692
Kabakum	−34.8239052	48.5119351	−14.7495889	−1.6685965	2.7900562	−0.8276108
Varna	−59.2623311	80.6677969	−24.4444979	−1.8938010	3.2049045	−0.9422916

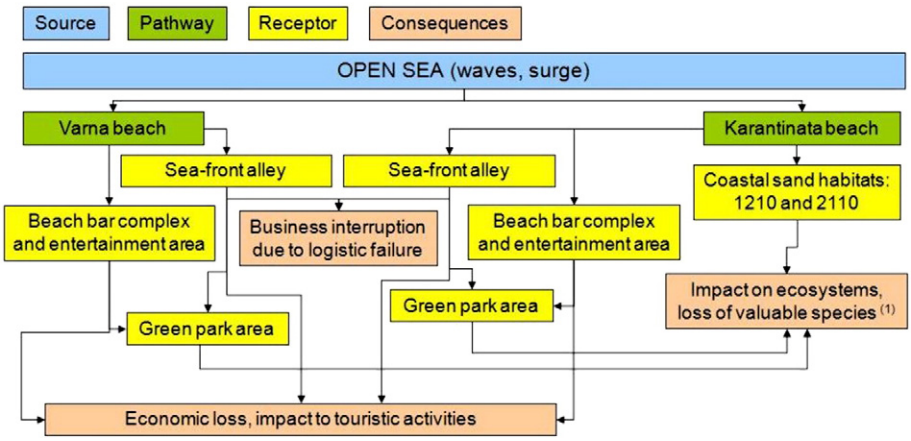

Fig. 9. SPRC analysis for Varna.

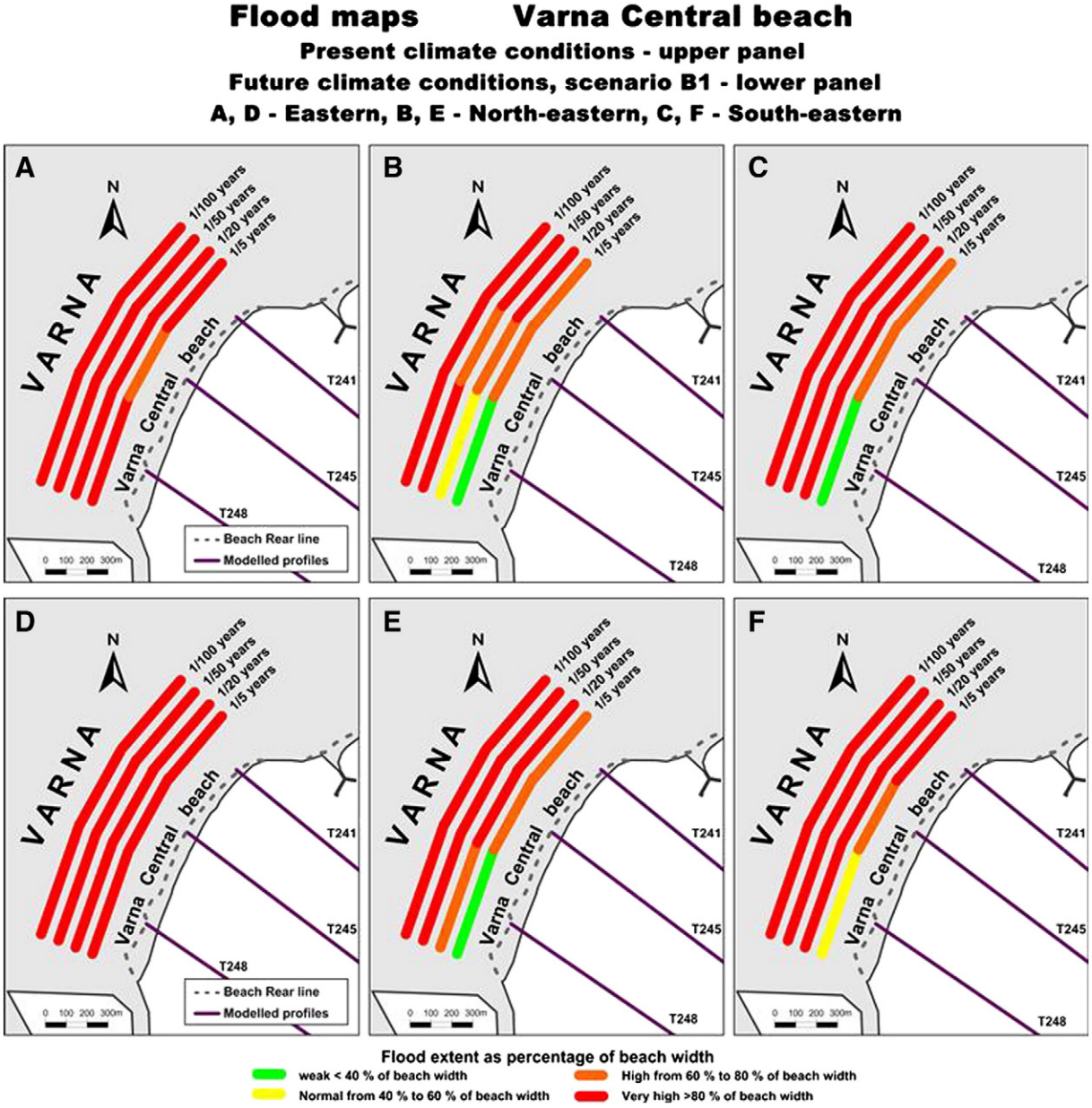

Fig. 10. Flood maps for E (panels A, D), NE (panels B, E) and SE (panels C, F) prototype storms for Varna beach for present (upper panels) and future scenario B1 (lower panels) climate conditions.

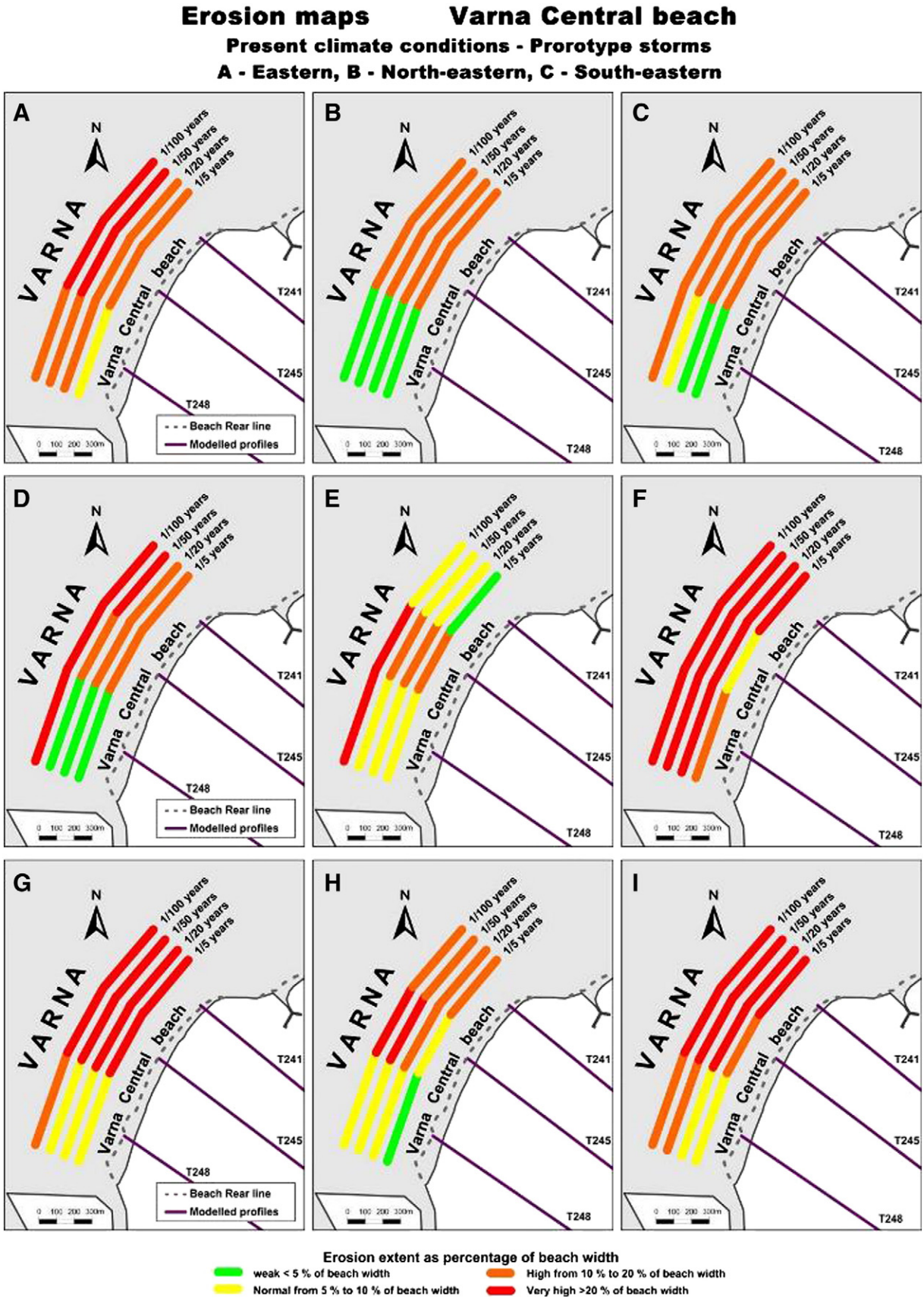

Fig. 11. Maps of erosion for E (panels A, D, G), NE (panels B, E, H) and SE (panels C, F, I) prototype storms for Varna beach. Results are from modelling by IO-BASMM (A–C), Xbeach (D–F), SBeach (G–I).

Table 6
Average and maximum beach erosion at Varna beach for eastern, north-eastern and south-eastern storms.

Model	Eastern			North-eastern			South-eastern		
	Average	Max	Profile	Average	Max	Profile	Average	Max	Profile
	m	m		m	m		m	m	
IO-BAS MM	5.9	6.9	T241	3.0	4.4	T245	5.3	7.2	T248
Xbeach	15.5	22.4	T248	8.1	12.0	T248	13.0	18.0	T248
Sbeach	7.8	9.2	T245	4.9	6.7	T245	7.6	10.4	T245

(6.9 m), while during NE and SE storms maximum erosion is foreseen at central and southern parts, respectively. The maximum erosion calculated by the Xbeach model is observed at the southern part of the beach (22.4 m), as the erosion caused by eastern storms surpasses that caused by north-eastern (12.0 m) and south-eastern (18.0 m). A characteristic feature of the results from SBeach is that the maximum erosion triggered by south-eastern storms (10.4 m) exceeds the magnitudes of erosion due to the eastern storms (9.2 m). For similar conditions Xbeach predicts greater erosion than SBeach and IO-BASMM.

General patterns of erosion for future climate scenarios remain similar to those for present climate. Northern and central parts of the beach are more vulnerable than the southern part. Minor differences in erosion maps reflect the fact that the wave magnitude for climate scenario B1 is increased in comparison to the A1B scenario.

Two historical storms: February, 1979 and March, 2010, were modelled to define flood patterns at four beaches during these storms. Time series of beach flooding for Golden Sands, Kabakum, Varna, and Karantinata during the storm of February 1979 are presented in Fig. 12. For comparison, time series of beach flooding for the same locations during the storm of March 2010 are also shown. In spite of the comparable maximum values of H_s and V during the storms, the significant difference in η_s (Table 5) is due to the considerable difference in duration of the stage of maximum storm development. During the storm of March 2010 Varna beach was flooded more than 40% of its width only for two hours, while during the storm of February 1979 it was flooded for 42 h.

Based on the analysis of all maps of erosion it can be concluded that maximum erosion due to eastern storms outmatches considerably that caused by the NE prototype storms for all four beaches. The approach, using flood and erosion maps is very useful when the manifestation of extreme phenomena is the focus of the analysis. However, the maximum run-up position is not an indicator of irrecoverable damage. In some conditions damage is a function of the flood duration. To investigate the nature/patterns of the connection between flood depth and duration, two hundred and twenty-four IDF curves were constructed based on model results: for two climate scenarios, four horizons (current state, short-tem, mid-term, and long-term), three wave directions, and for ten profiles. In Fig. 13 an example of such a graph for climate scenarios A1B and B1, mid-term horizon for Profile T248 (southern part of Varna Central beach) is presented.

Differences in flood intensity between A1B and B1 climate scenarios are insignificant. As a whole, flood scenarios related to B1 are more severe than those of A1B, which is a consequence of rougher wave forcing. For instance, during an eastern storm with $T_r = 100$ years (A1B scenario, mid-term horizon) all objects located below 3 m MSL would be flooded for at least 30 h, while for the B1 scenario, they would be flooded for 36 h (Fig. 13).

4. Spanish case study: Long-term trends of extreme flooding and erosion in santander

4.1. Site description

The study of this site focuses on the definition of sources and hazards and their statistical characterisation in specific locations along the coast of Santander Bay, Northern Spain. This area is one of the largest inlets on the Cantabrian Coast (2270 ha) and is characterised by several morphodynamic elements (Fig. 14): Sardinero, Loredo and Somo beaches, outside the bay, Magdalena-Peligros and Puntal beaches, in the spit, and the bay. Since the 18th century, and due to the development of the city of Santander, the bay has suffered many changes which have determined the evolution of the morphodynamic system. The land required for the expansion of the city was obtained from the bay by reclaiming its western part resulting in a subsequent decrease of the tidal prism. Besides, intensive dredging activity, mainly on the offshore shoal and in the spit end, has been carried out in order to maintain a navigable channel.

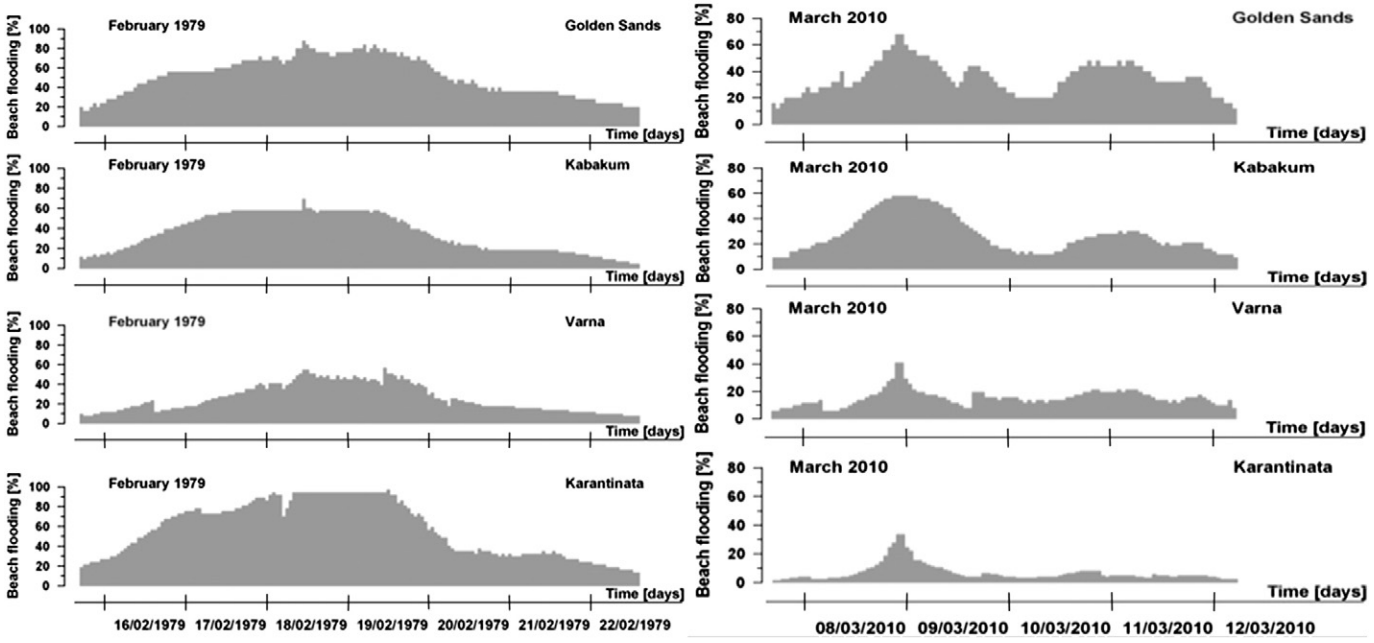

Fig. 12. Flooding of 4 beaches—Golden sands, Kabakum, Varna, and Karantinata during the storm of February 1979 (left) and March 2010 (right).

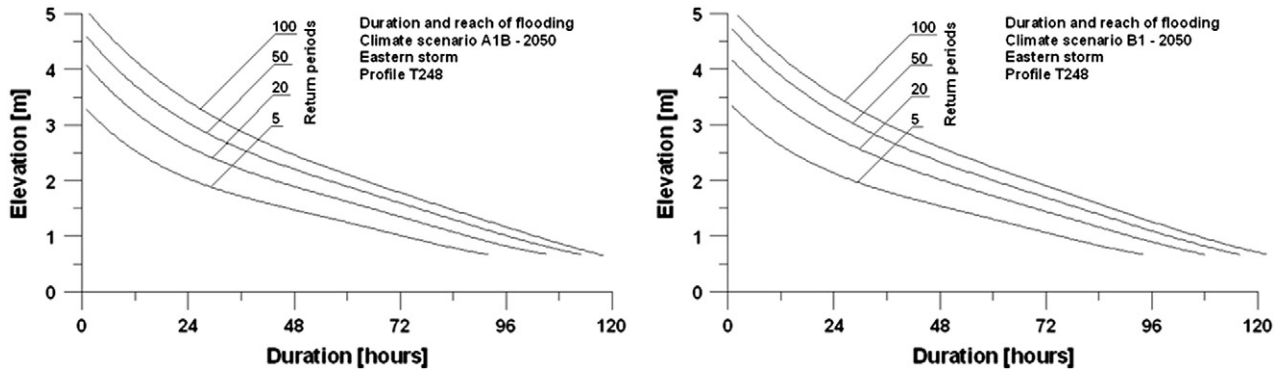

Fig. 13. Intensity–Duration–Frequency curves for eastern storm and for Varna Central beach.

The complexity and historical evolution of Santander spit requires care in the definition of sources for each element of the coastline. Fig. 15 presents a SPRC scheme relative to Santander, with the purpose of identifying the main conceptual units within the site.

4.2. Data

The main sources considered in this analysis are the marine dynamics, including waves and sea level. For this, several data sets, numerical modelling and statistical techniques are used and explained below.

4.2.1. Wind data

In this work, we have used the 10 m wind fields from the global reanalysis NCEP/NCAR (with spatial resolution 1.9° and temporal resolution 6 h, Kalnay et al., 1996) as inputs to define the wave conditions in the Atlantic and Cantabrian Sea.

4.2.2. Wave data

The global wave hindcast GOW (Reguero et al., 2012) was used to carry out this study. The wave model used was Wavewatch III (Tolman, 1999), forced by 6-hourly wind fields from the atmosphere model NCEP/NCAR. The reanalysis GOW spans from 1948 onwards with hourly resolution. A limitation of the model is that it is not able to simulate propagation effects in shallow waters as effectively as other models. Consequently, results from simulations of the Wavewatch III have been used as initial conditions in the simulations of the propagation model SWAN (Booij et al., 1999), increasing the spatial resolution.

The reanalysis data from GOW have been calibrated using altimeter data from six different satellite missions for the period between 1992 and 2010: TOPEX, Jason-1, Jason-2, Envisat, GFO and ERS-2 (http://www.aviso.oceanobs.com/). The calibration procedures summarised in Woolf et al. (2002), and later updated by Hemer et al. (2010), have been applied to the altimeter significant wave height (H_s).

After propagating the wave climate into shallow waters the results were validated using buoy data. The shallow water buoys Virgen del Mar and Santoña, from the Cantabrian network Red Vigia (Consejería de Medio Ambiente, Gobierno de Cantabria), and the Bilbao buoy from the shallow water network (REDCOS) from Puertos del Estado (OPPE, Ministry of Public Works, Spain) have been used.

4.2.3. Sea level data

We used hourly time series from two different tide gauges, namely from the Spanish Institution of Oceanography (1940–2005) (IEO) and from Puertos del Estado (1995-present) that provide astronomical and the residual tides. In order to fill the gaps of the instrumental time series of non-tidal residuals, storm surge reanalysis data from the model GOS, developed by IH Cantabria, were used (Abascal et al., 2010). The reanalysis model GOS (Global Ocean Surge) is forced by a 60 year dynamic atmosphere downscaling (SEAWIND, IH Cantabria) with 30 km spatial resolution.

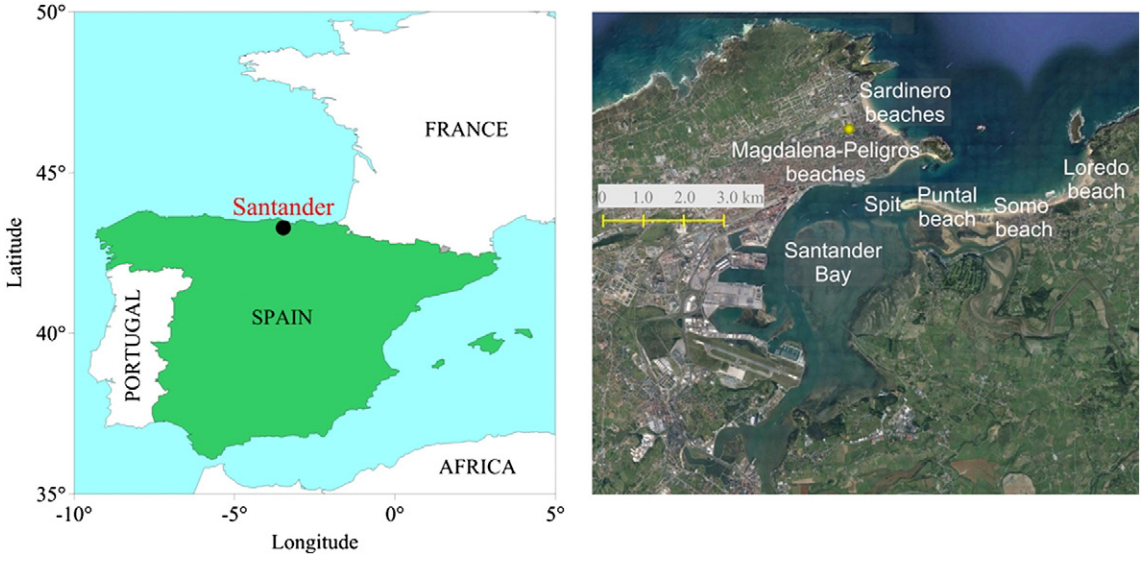

Fig. 14. Location and considered elements in the Bay of Santander.

4.3. Methodology: Downscaling marine dynamics

The study of different processes in the coastal area requires the propagation of marine dynamics into shallow waters (Camus et al., 2011). In this study, we follow the approach summarised in Fig. 16, based on seven steps. To have long-term temporal and spatial wave data coverage to properly characterise wave climate requires the use of reanalysis data (1), in this case the data base GOW. Numerical data requires calibration in order to correct the numerical model limitations (2). We used the directional calibration methodology explained in Mínguez et al. (2011). Moreover, numerical models of wave generation from atmospheric forcing do not simulate propagation effects in shallow waters, therefore, reanalysis data in deep water must be transferred into shallow waters using statistical or dynamical downscaling. In order to minimise the propagation task (over 500,000 hourly sea states in a 61-year wave reanalysis) we used mathematical algorithms which are able to select a reduced number of representative sea states of the wave climate in deep waters (3) (Camus et al., 2011). Once the sea states were selected, we propagated them using the SWAN numerical model to determine wave characteristics at the objective points along the coast (4). Using the results of the propagated sea states and interpolation techniques we reconstructed time series of the required wave parameters for the assessment of flood and erosion events (5). Finally, using wave data from coastal buoys, we validated the results of wave parameters obtained combining the statistical and dynamical downscaling (6). After that, marine dynamics were transferred into shallow waters, and the analysis of coastal marine climate and other coastal processes could be carried out (7).

4.3.1. Definition of the hazard: Flooding and erosion

In the context of this case study, the hazards that affect the impact units I_i through the pathways are the flooding and episodic or non-permanent erosion in our study area. Therefore, the goal is to statistically characterise the distributions $f_z(z)$, both in intensity and frequency, where z is the random variable that defines the intensity of the hazard. To that purpose, we established 10 homogeneous units based on similar characteristics of mean H_{s12}, mean energy flux and mean direction (Fig. 17). The clustering of these areas was achieved using the Self-Organizing Maps (SOM) technique (Kohonen, 2000). This classification technique detects common patterns in the data and projects them onto a dimensional lattice, which adapts to the data using nearest neighbour optimisation. We selected six points in the main beaches of the domain: two points in Sardinero beaches, three points in Loredo, Somo and Puntal beaches and another one inside the Bay, in Peligros beach (see Fig. 17).

4.3.1.1. Flooding. The flooding hazard is characterised through the flooding level which is defined as the result of the addition of four factors: mean sea level (*MSL*), astronomical tide (*AT*), storm surge (η_s) and run-up ($R_{u2\%}$):

$$FL = MSL + AT + \eta_s + R_{u2\%}. \tag{6}$$

Monthly mean sea level is calculated using the long-term tidal gauge free surface record (1948–2009) from IEO. The astronomical tide is obtained from the Santander tide gauge (REDMAR, Puertos del Estado). The storm surge is a random variable which consists of variations in the sea level due to wind and pressure variations. The time series of storm surge in this study comes from merging the Santander tide gauge from IEO and the numerical model GOS. Finally, the run-up is the elevation of the water surface due to the action of waves (with reference to the remaining sea level). After the wave breaking, the energy that has not been dissipated during the breaking process elevates the water surface along the berm of the beach. In this study we used the formulation from Nielsen and Hanslow (1991). Results reveal that in the case of dissipative beaches there is no dependence between run-up and beach slope ($\tan\beta < 1/10$), while in the case of reflected beaches there is a dependence with the slope, and therefore, with the Iribarren number:

$$\begin{aligned} z &= 0.47(H_s L_\infty)^{0.5} \tan\beta \quad \tan\beta > 0.1 \\ z &= 0.04(H_s L_\infty)^{0.5} \quad \tan\beta < 0.1 \end{aligned} \tag{7}$$

$$R_{u2\%} = 1.98z \tag{8}$$

where $R_{u2\%}$ is the run-up exceeded 2% of the time every sea state (1 every 50 waves). We have calculated the hourly time series of flooding level in each objective point.

4.3.1.2. Extreme erosion events. In this study we use the empirical approach developed by Miller and Livermont (2008) which defines the Peak Erosion Intensity (PEI) Index as a function of the local wave height

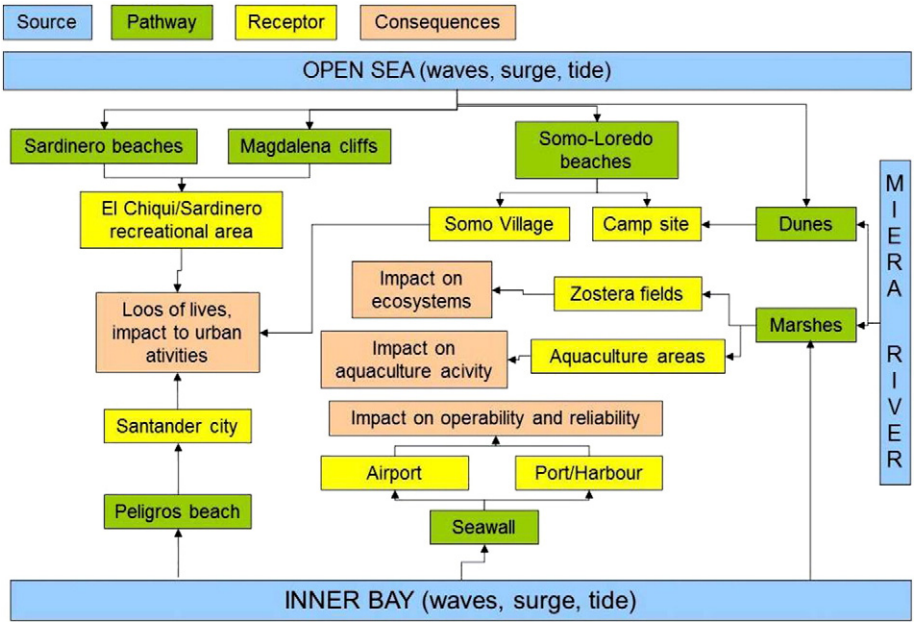

Fig. 15. SPRC analysis for Santander.

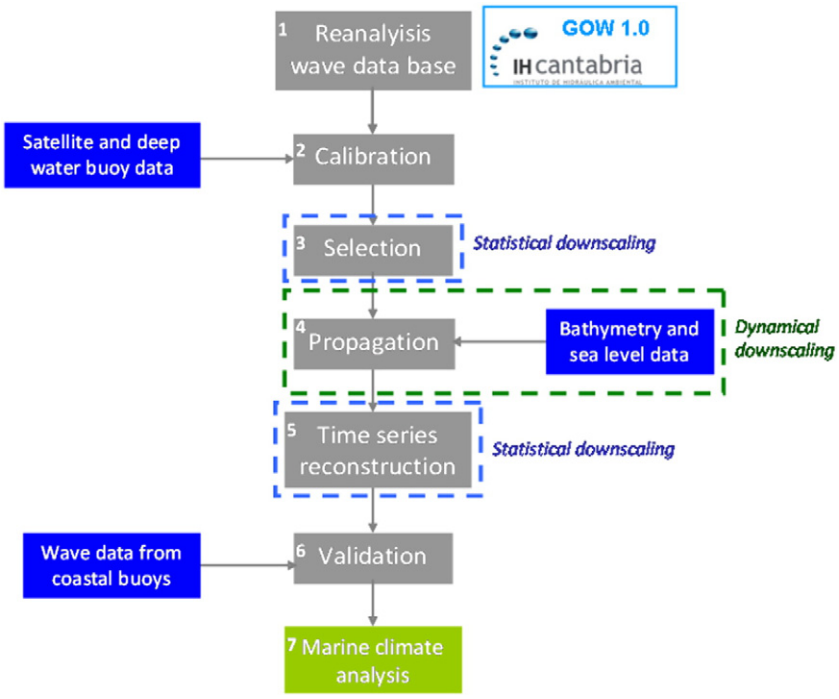

Fig. 16. Methodology for downscaling wave climate to coastal areas.

(H_b) and the total sea level (S). The PEI index, or equivalently the equilibrium shoreline change is defined as:

$$PEI(t_i) = W_*(t_i)\left[\frac{0.068H_b(t_i) + S(t_i)}{B + 1.28H_b(t_i)}\right] \quad (9)$$

where $W_*(t_i)$ is taken as the distance to the depth limited breakpoint, $h_*(t_i) = h_b(t_i) = 0.8H_b(t_i)$. $S(t_i)$ is the water level variation across the surf zone. The berm height B is assumed to be constant over time. Note that water levels are relative to MSL and include both the astronomical and surge component. Following this formulation, the PEI hourly time series are obtained at the different objective points.

4.3.2. Statistical modelling of the hazard

The simplest model in extreme value theory is the Annual Maxima method (Coles, 2001), which uses only annual maxima values. This is

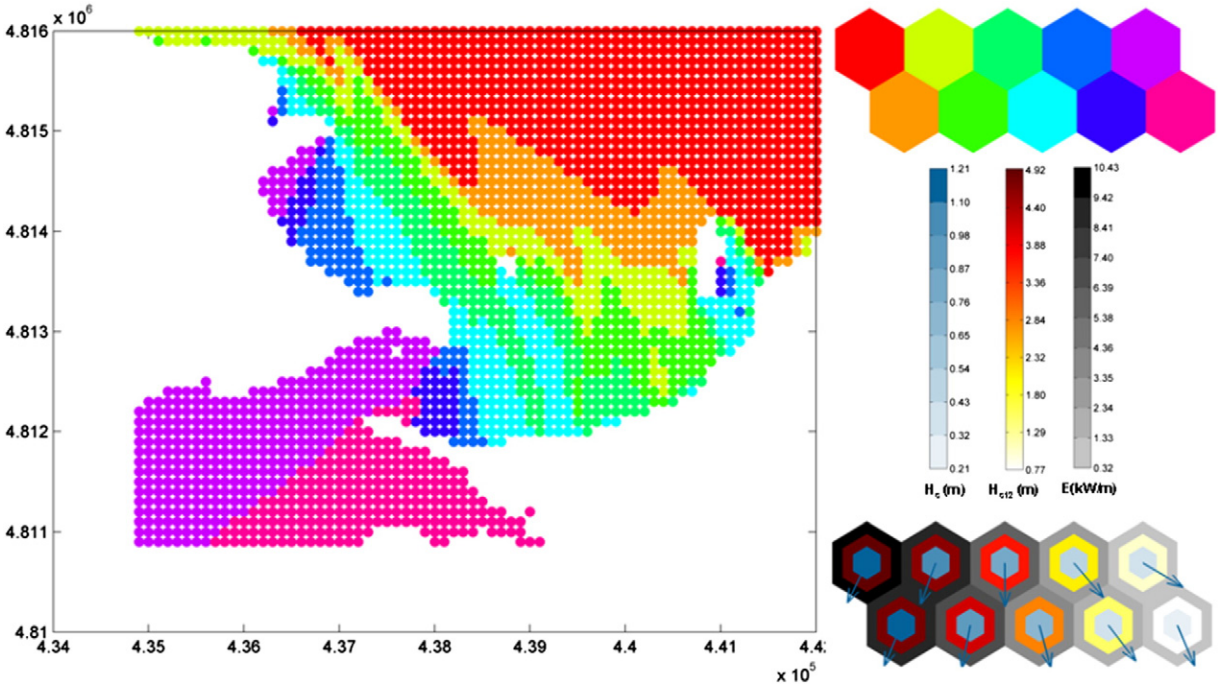

Fig. 17. Classification of Santander Spit by similar zones of wave characteristics. Each group defined by a colour has certain conditions of significant wave height, significant wave height only exceed 12 h a year, energy and mean direction.

modelled using the generalised extreme value distribution (GEV) cumulative distribution function (CDF) given by:

$$F(x;\mu,\psi,\xi)=\begin{cases}\exp\left[-\left(1+\xi\frac{x-\mu}{\psi}\right)^{-1/\xi}\right] & \xi\neq 0\\ \exp\left[-\exp\left(-\frac{x-\mu}{\psi}\right)\right] & \xi=0\end{cases} \quad (10)$$

where $1+\xi(x-\mu)/\psi>0$, μ is a location parameter, ψ is a scale parameter and ξ is the shape parameter which determines the nature of the tail of the distribution. An important problem in extreme value analysis is the scarcity of data for model estimation. To mitigate this problem, we use the peak over threshold (POT) method for independent and identically distributed random variables. The basic idea is to pick up a high threshold u and to study all the exceedances over u, assuming that the number of exceedances in any given year follows a Poisson distribution with mean ν and which the excess values $y=x-u$, modelled using the generalised Pareto distribution (Pickands, 1975) given by:

$$G(y;\sigma,\xi)=\begin{cases}1-(1+\xi y/\sigma)^{-1/\xi} & \xi\neq 0\\ 1-\exp(-y/\sigma) & \xi=0\end{cases} \quad (11)$$

where $\sigma>0$ is a scale parameter and ξ is the same shape parameter as in the GEV distribution. The combination of both models for frequency and intensity can be expressed in terms of the GEV parameters for annual maxima provided that $\sigma=\psi+\xi(u-\mu)$ and $\nu=(1+\xi(u-\mu)/\psi)^{-1/\xi}$. Moreover, the hypothesis of homogeneity in the random variable y can be relaxed to model non-stationarity, as seasonal effects or long-term trends. Therefore, an extension of the GPD-Poisson model is obtained by allowing its parameters to be time-dependent, so that $\nu(t)>0$, $\sigma(t)>0$ and $-\infty<\xi(t)<\infty$ may vary throughout the year. Accordingly, the GEV distribution has time-dependent parameters, for example, which may contain sine waves representing seasonal effects (see Méndez et al., 2006). Likelihood-based methods allow modelling different factors to explain the variability of the data and the non-stationarity of the GEV and GPD-Poisson parameters. Among these factors, we shall consider the annual variability (seasonality), the likely long-term trend, and other cycles such as the nodal cycle for astronomical tide. We express the model in terms of the GEV parameters using the time-dependent version of Eq. (9) to relate the GPD-Poisson parameters to the equivalent GEV parameters. A number of possible regression models can be expressed in terms of the time-dependent location, scale, and shape parameter of the GEV distribution. In the following paragraphs, we will show the regression model including seasonality (in location and scale parameters) and the long-term trend as an additional term in the location parameter.

$$\mu(t)=\beta_0+\beta_1\cos(2\pi t)+\beta_2\sin(2\pi t)+\beta_3\cos(4\pi t)+\beta_4\sin(4\pi t)+\beta_{LT}\cdot t \quad (12)$$

$$\psi(t)=\alpha_0+\alpha_1\cos(2\pi t)+\alpha_2\sin(2\pi t)+\alpha_3\cos(4\pi t)+\alpha_4\sin(4\pi t) \quad (13)$$

$$\xi(t)=\xi_0 \quad (14)$$

where β_0, α_0 and ξ_0 are mean values and, β_{LT} represents the annual mean trend, and t is given in years.

4.4. Results

We analysed flooding and erosion hazards in Santander spit, obtaining the present climate statistical distribution and its long-term trend in the last 62 years.

4.4.1. Flooding

The time series of the flooding level (FL) in the six objective points were obtained. The intensity of the flooding levels depends on the exposure of the beach, and therefore, on the energy received. The most energetic beaches are Loredo and Somo, which face north and receive almost directly the most energetic swells from the NW diffracted in Cabo Mayor Cape. In the case of Loredo beach, some sea states reach 10 m of flooding level. Puntal and Peligros, which are sheltered by La Magdalena peninsula and are located at the entrance of the bay, registered the lowest flooding levels. In order to characterise the extreme flooding climate the statistical model Pareto–Poisson described above was applied. This statistical model is based on the maxima selection peak over threshold (POT) method. Based on previous studies in the area, the threshold u was the flood level corresponding to the 98 percentile (i.e. $u_{Loredo}=6.89$ m). An interdependency of three days between storms was used. The application of the stationary model provides the extreme flooding climate in each point for different return levels. After that, the non-stationary model was carried out. The seasonality was modelled including harmonic functions in the location and scale parameter and the long-term trend by adding a linear term in the location parameter. The long-term trend is only included when significant at a 0.1 confidence level. It is significant at all locations with values around 0.2 cm/year. Fig. 18 shows the time series of flooding level in Loredo beach and the cumulative distribution function in present time (2010) and in 2050, obtained by extrapolating the long-term trend (β_{LT} =0.3 cm/year).

Concerning the cumulative distribution function, it can be seen that the statistical characterisation of flooding level changes in the future, due to the positive long-term trends. Assuming that β_{LT} is constant in the period 2010–2050, it can also be seen that the probability of occurrence of flooding levels increases in 2050 (see example of Fig. 18). For example, the probability of an exceedance of 7.2 m of the annual maxima flooding level in 2010 is 0.6 while this probability in 2050 reaches 0.8. In terms of return period, the event occurring once in a 100 years reaches 9 m in 2010, while in 2050 this flooding level corresponds to 8.14 m (approximately 0.8 m lower). Similar results are found for the rest of the beaches since significant positive trends are found.

4.4.2. Erosion

The erosion study was carried out on the six points selected along the beaches. We obtained the Peak Erosion Intensity (PEI) index hourly time series at each point. Agreement results with the flooding level time series are found. Loredo is the beach with higher erosion episodes as it is exposed to the most energetic sea states, reaching 50 m of berm erosion in 1965. Similar analysis to flooding levels was performed to characterise extreme erosion climate. First, the stationary extreme model Pareto-Poisson was fitted. The threshold, u, selected to identify PEI exceedances was the $PEI_{98\%}$: $u_{Sardinero2}=12.67$ m, $u_{Sardinero1}=11.95$ m, $u_{Loredo}=18.80$ m, $u_{Somo}=14.90$ m, $u_{Puntal}=10.11$ m and $u_{Peligros}=7.24$ m. Again, an interdependency of three days between storms has been used. In the case of flooding, the shape parameter takes negative values (Weibull distribution), with a bounded tail, while in the case of erosion, the shape parameter values are also negative but very close to 0, signifying a Gumbel distribution and light tail (see example of Fig. 19). For example, the quantile of PEI associated to 50-year return period corresponds to 45 m in Loredo.

Once the stationary extreme erosion climate is characterised we have fitted the non-stationary Pareto-Poisson model in order to assess variability throughout the year and in the long term. Only a significant long-term trend is detected in Peligros beach. Using the Pareto distribution, we modelled the intensity of the exceedances of PEI index and using the Poisson model we analysed the frequency of erosion events (Fig. 20). Note that in the most exposed beaches, the annual cycle is clear and predominant. Regarding the frequency, the maximum erosion rate occurs in November–December, which means the importance of the semi-annual cycle, particularly in the autumn months. The highest erosion rate can be found in Sardinero beaches and Puntal.

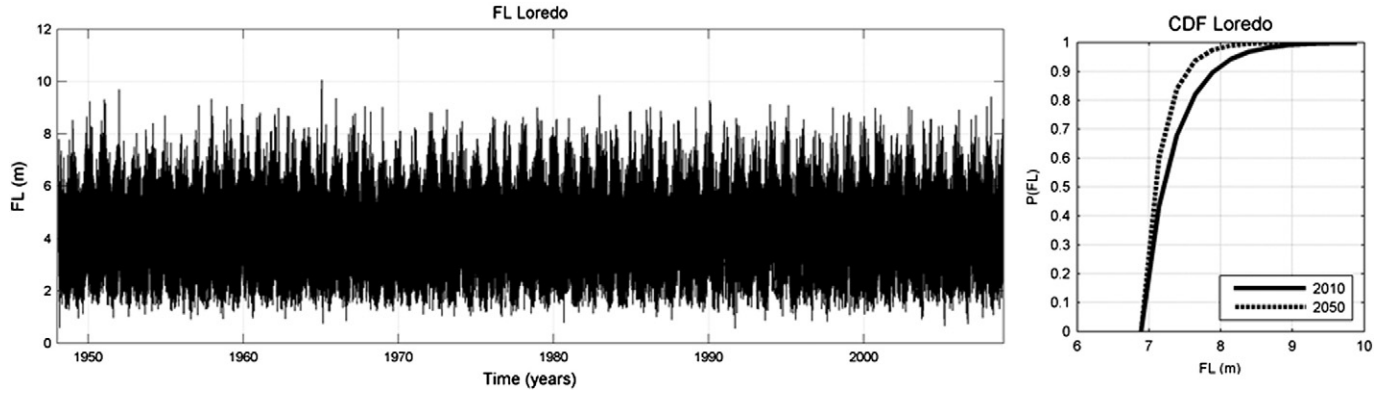

Fig. 18. Flooding level time series for Loredo beach (left panel) and its cumulative distribution function currently (2010, continuous line) and in 2050 (dashed line).

5. United Kingdom case study: Present and future flooding from plymouth sounds to exe estuary

5.1. Site description

The UK study site is from Plymouth Sound to Exe Estuary, which is located in southwest England, as shown in Fig. 21. The area encompasses a 100 km stretch of coastline bordered by the English Channel. It is one of the most diverse coastal settings in Europe, incorporating a range of habitats from exposed rocky and shingle coast to sheltered mud of flooded valleys or "Rias" together with densely populated urbanised and industrial zones of Plymouth Sound and Torbay. Therefore, it is a unique and representative site to involve the complex coastal and estuarine processes and the interaction between coastal defence structures and coastal morphology.

Within the study site, the research is focused on the Teign Estuary (Fig. 21c). A major modifier of the coastline is the railway line, which occupies considerable stretches of coastal frontage (from Exeter to Dawlish to Teignmouth to Newton Abbot). Coastal defence work to protect the railway line has modified coastal processes. Pressures also include physical disturbance, for example by trampling, dredging, fishing gear, land reclamation and adjacent coastal development, construction of sea defences and potential for changes in the hydrological regime.

The spring tidal range at the study site is 3.8 m, with a maximum tidal current of 3.0 m/s, although the tidal current in the Lyme Bay is relatively weak, of 0.5 m/s in general. The waves in the area are predominately swell waves from the Atlantic in the southwesterly direction, with yearly mean significant wave height of 2.0 m (max 4.0 m) and 2.7 m for a 50 year return period (max 5.3 m).

The River Teign arises on Dartmoor at a height of 520 m AOD (above Ordinance Datum at Newlyn) and flows in a southeasterly direction towards the Teign Estuary and the sea. The catchment covers an area of 550 km^2. The principal sub-catchments are the Rivers Lemon and Bovey and the Aller Brook. The estuary is also influenced by the large river flow. The River Teign flows through a diversity of landscapes and habitats, ranging from open moorland (Dartmoor) to ancient woodland, improved pasture land and broad valleys, before finally meeting its floodplain and the estuary. The Teign Estuary is approximately 9 km in length and less than 1 km wide at its widest Point and is defined as a Ria by JNCC (1997). It is one of South Devon's most valuable assets. The mouth of the Estuary is marked by a permanent spit "the Point", on the north bank at Teignmouth extending southwest, and the red cliffs at Shaldon to the south.

Fig. 22 presents a large-scale SPRC scheme relative to Teign Estuary, with the identification of the main units of sources, pathways, receptors as well as the possible consequences within the individual study sites. The main sources within this site are from the open sea, i.e. the English Channel with waves, tides and storm surge, and the flooding water from River Teign in the upstream. The local wind generated waves and water level setup can be significant sources in the area. The main pathways (which may also be considered as receptors of lower intrinsic value) include sea wall, groynes, revetment/beaches and marshes, where the main receptors (that may also be pathways for other receptors) are the mainline railway, towns and industrial, commercial and ecology-significant areas. The possible consequences are also illustrated in the figure.

The small-scale analysis evaluates the actual proximity of the receptors from the sources, by studying the flood dynamics, erosion maps, effectiveness of the coastal structures (submerged breakwaters and groynes) and mitigation measures for ecological impacts.

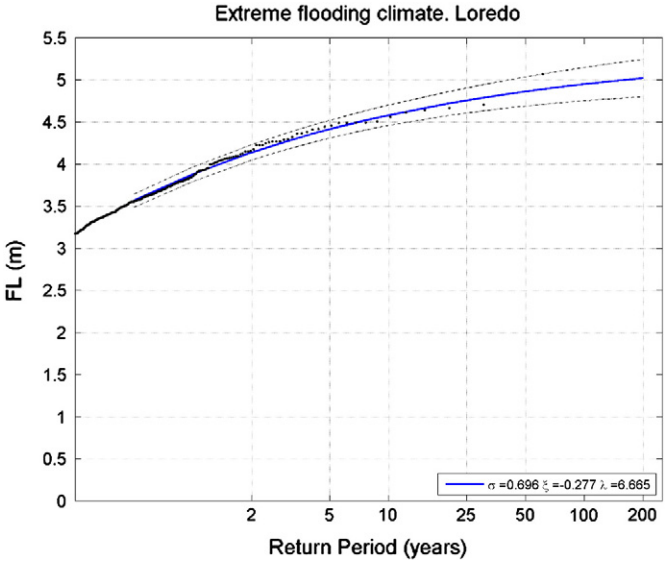

Fig. 19. Extreme erosion in Loredo beach.

5.2. Data

For the present climate conditions analysis, various data sources have been used, detailed as follows:

- Tides and surge:
  - Data: the British Oceanographic Data Centre (BODC — www.bodc.ac.uk)
  - Locations: Devonport and Weymouth, two closest tide gauge stations to the study site
  - Time series of tidal and surge levels (15-min intervals) and monthly extremes (maxima and minima) and monthly mean water levels
  - Duration: 1991–2009

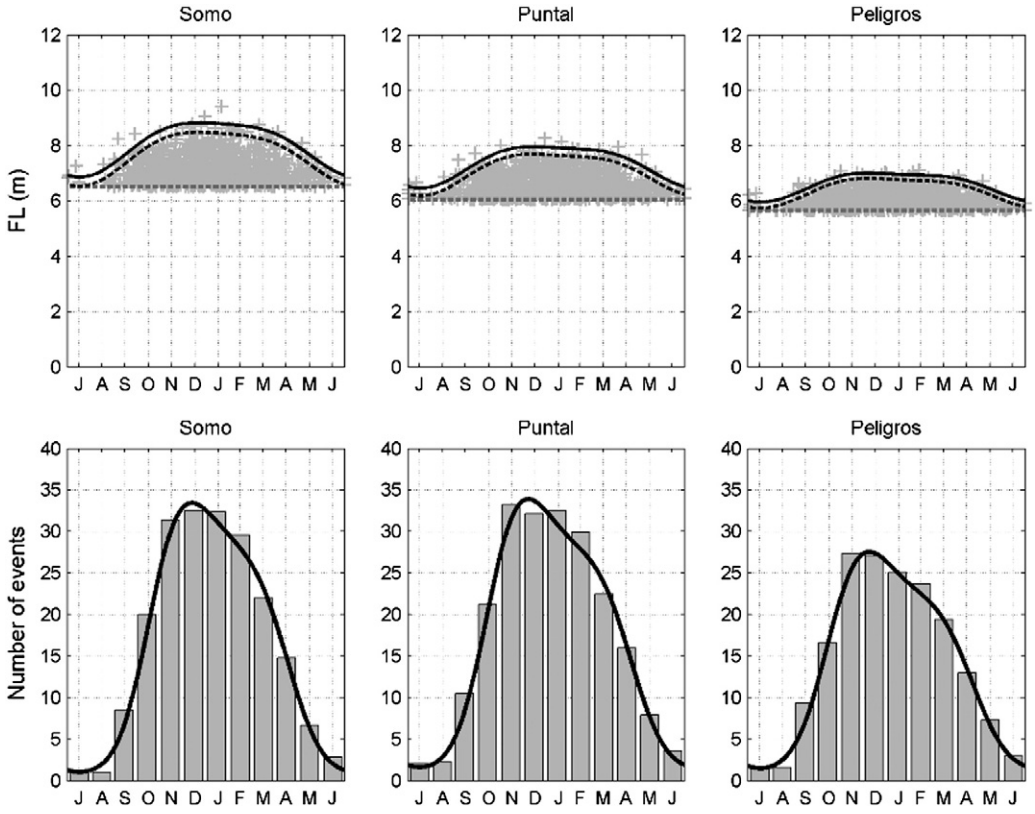

Fig. 20. Upper panels: Annual evolution of location (solid line) and location + scale (dashed black line), and 98% exceedances over the threshold (dashed grey line). Lower panels: Histogram of the time of occurrence of threshold excesses (bars) and time-dependent event rate within a year in an average year (solid line), according to the fitted model.

- Waves:
  - No measured wave data available in the study site
  - Model results from POLCOMS, forced by the wind data from ECMWF database
  - Locations: Devonport & Exe/Teign Estuaries
  - Duration: 1970–2000
- River discharge:
  - Data from National River Flow Archive, UK
  - Location: River Teign at Preston (station ID: 46002)
  - Duration: 1956–2007 (daily).

In general, the extremes were calculated by fitting the annual maxima to a selection of candidate probability distribution functions.

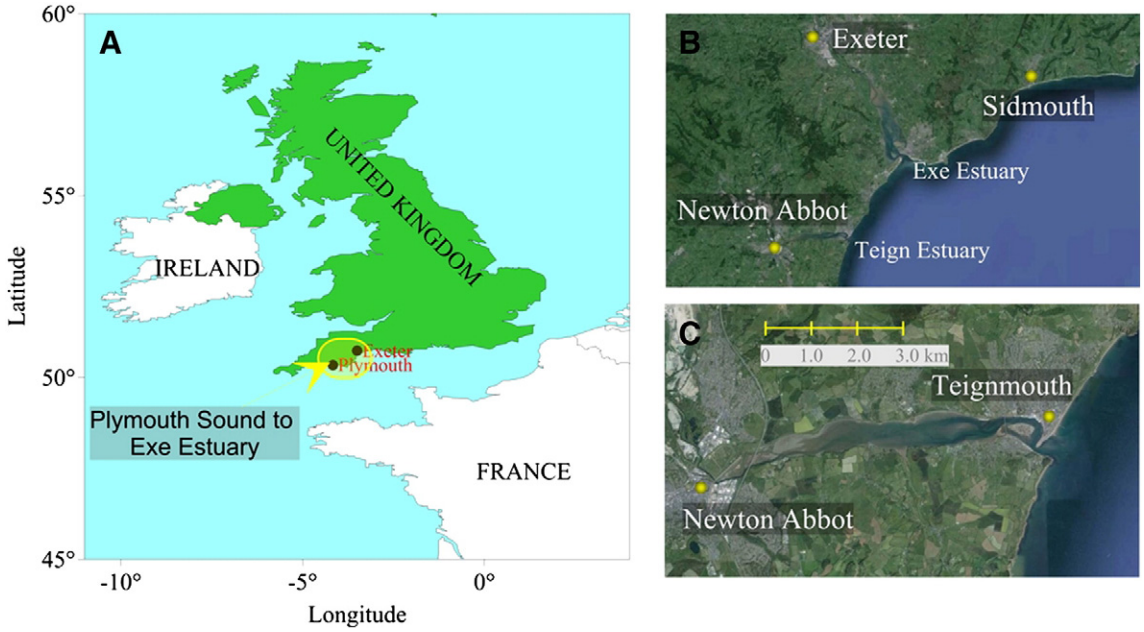

Fig. 21. (A) Plymouth Sound to Exe Estuary, (B) Exe and Teign Estuaries, and (C) Teign Estuary.

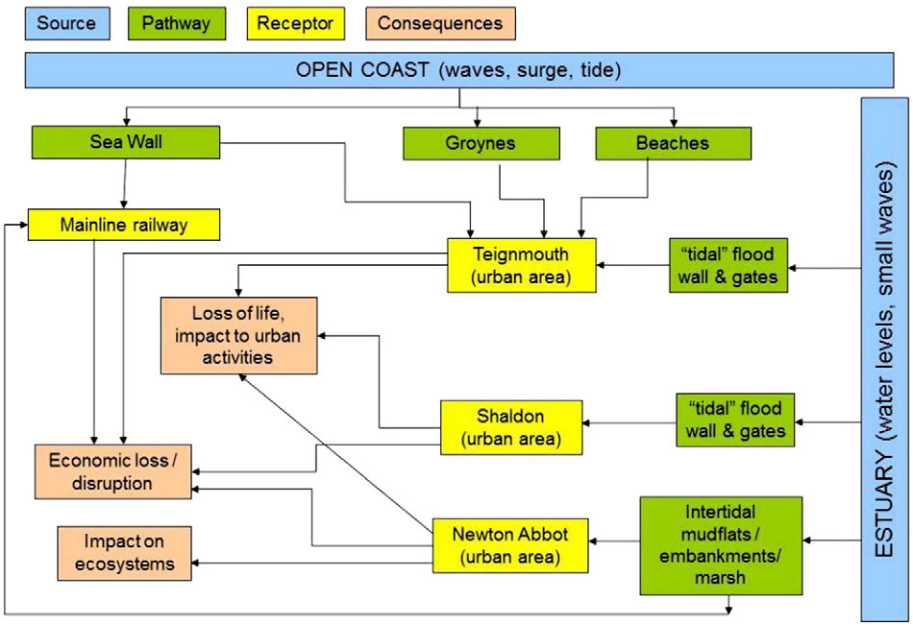

Fig. 22. SPRC analysis for Teign Estuary.

The 1-year lag correlation was calculated to ensure statistical independence within the time series. Given the time-limited extent of the data sets, bootstrapping was used to re-sample the data and generate confidence limits based on the re-sampled populations following the methods described in Reeve (1996) and Li et al. (2008).

To extend the field measurement data, a nested POLCOMS/ProWAM modelling system (Holt and James, 2001) was setup from the northern Atlantic Ocean with its coarser grid, to the English Channel with its finer grid, to compute waves and storm surge for the present (1970–2000) and the future scenarios (2010–2100). The model has been extensively tested and validated in the area (Chen et al., 2010; Pan et al., 2009).

5.3. Methodology: Scenario construction

5.3.1. Mean sea level

The measured mean sea levels at the tidal gauges closest to the study site, Plymouth (Devonport) and Weymouth are analysed. The average water level at Plymouth is 3.29 m above Chart Datum (CD) (0.07 m AOD) and 1.27 m above CD at Weymouth (0.34 m AOD). The yearly averages of the mean water levels indicate a tendency of a slight increase at both Plymouth and Weymouth in the range of 10 cm over the past 20 years. The mean sea level increase is more steadily at Plymouth than that at Weymouth. The results also show that the yearly maxima and minima of the measured sea levels from 1990 to 2009 are both around 1.0 m AOD at Plymouth (Devonport) and Weymouth. The results indicate that the high water levels fluctuate slightly over this period at both locations.

The measured surge levels, after the tidal components being removed from the measured water levels, over the same period are also analysed. At Plymouth, the storm surge was higher during 1992 and 1993, up to 1 m, and then decreased to 0.6 m for the following few years. Since then, the surge level has a tendency to increase, from 0.6 m to 0.8 m in recent years. Yearly maximum surge levels at Weymouth have been constant, at around 1 m. In 2008, the surge level exceeded 1 m.

5.3.2. Return values of tides and surge

Measured tide and surge levels were analysed using Weibull, Gumbel and bootstrapping methods. The maximum and minimum extreme water levels for 2, 5, 10, 20, 50, 100, 200, 500, 1000 and 2000 year return periods at both Plymouth and Weymouth are predicted using both Weibull and Gumbel distributions, the results of which in general agree. However, due to the lower/higher limits required in using the Weibull distribution, the former results are believed to contain a further uncertainty. Therefore, all predicted extremes using the Gumbel distribution are used in the extreme analysis hereafter.

At Plymouth, the extreme water level is likely to increase approximately by 1 m for 1 in 2000 year events. At Weymouth, such an increase is also found, in the range of 0.8 m. The extreme analysis has also been applied to the storm surge level at Plymouth and Weymouth. With the Gumbel distribution, the extreme surge level at Plymouth can be as high as 1.6 m in 1 in 2000 year return period events, while at Weymouth, the extreme surge level can reach more than 2 m. Table 7 gives the detailed extreme values for the maximum water and surge levels at Plymouth and Weymouth, for various return periods.

5.3.3. Joint distribution of waves & surges

For the joint distribution analysis, wave and surge data were obtained from the POLCOMS/ProWAM model, which was set up with nested grids centred at the study area. The present conditions were modelled using wind and sea level pressure (SLP) data from the European Centre for Medium-Range Weather Forecasts (ECMWF) for a 30 year period, from 1970 to 2000. Since the predominant waves are from the southwest, the maximum wave heights at Plymouth are generally higher than those at Exmouth, which is more sheltered to the waves from the southwest (Horrillo-Carballo et al., 2012). The highest wave height at Plymouth is 11.34 m and 8.14 m at Exmouth. The average wave heights over the 30 year period are 7.82 m and 5.81 m, at Plymouth and Exmouth respectively.

Table 7
Maximum water and surge levels (m AOD) for given return periods at Plymouth and Weymouth.

Return period (Years)	Plymouth (m AOD)		Weymouth (m AOD)	
	Max water level	Surge	Max water level	Surge
5	6.283	0.860	2.932	1.189
20	6.465	1.036	3.101	1.435
50	6.581	1.147	3.208	1.592
100	6.667	1.231	3.289	1.710

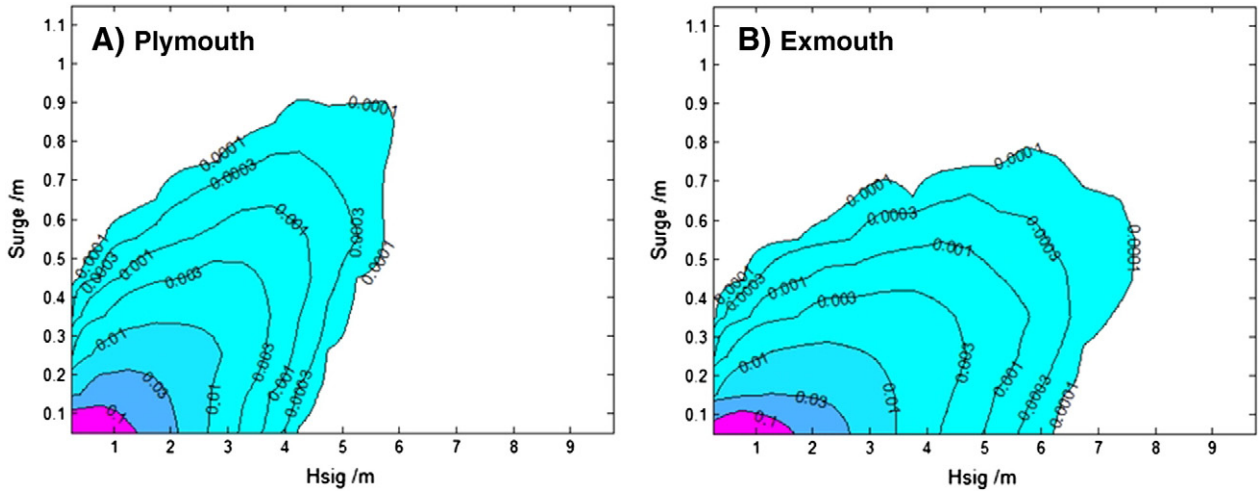

Fig. 23. Joint wave and surge distributions at Plymouth and Exmouth (contours in log scale).

The hourly wave heights and surge levels from the POLCOMS/ProWAM model have been divided into 0.25 m and 0.1 m intervals for the joint distribution analysis. The joint distributions of waves and surge at Plymouth and Exmouth are shown in Fig. 23. The results indicate a clear correlation between waves and surge at both locations. However, at the Exmouth location, the surge depends more strongly on the wave conditions. Based on the tidal gauge measurements, the most dangerous extreme sea level recorded at Plymouth occurred in 2004 and was 6.35 m (above CD − 3.13 m AOD), and the highest sea level recorded at Weymouth is 3.04 m (above CD − 2.11 m AOD) and occurred in 2008.

5.3.4. Future scenarios

Future scenarios were considered according to IPCC scenario A1B (IPCC, 2007), and the wind and SLP data from Max Planck Institute for Meteorology WDCC/CERA database (WDCC, 2009). Three time slices from 2010 to 2100 were modelled. Fig. 24 shows yearly maxima of significant wave heights at Plymouth and Exmouth, together with those under the present conditions.

The mean significant wave heights at Plymouth and Exmouth for 3 future time slices, together with those for the present conditions are shown in Fig. 25. At both locations, the mean significant wave heights under A1B scenarios for future time slices exhibit a cyclic pattern. The

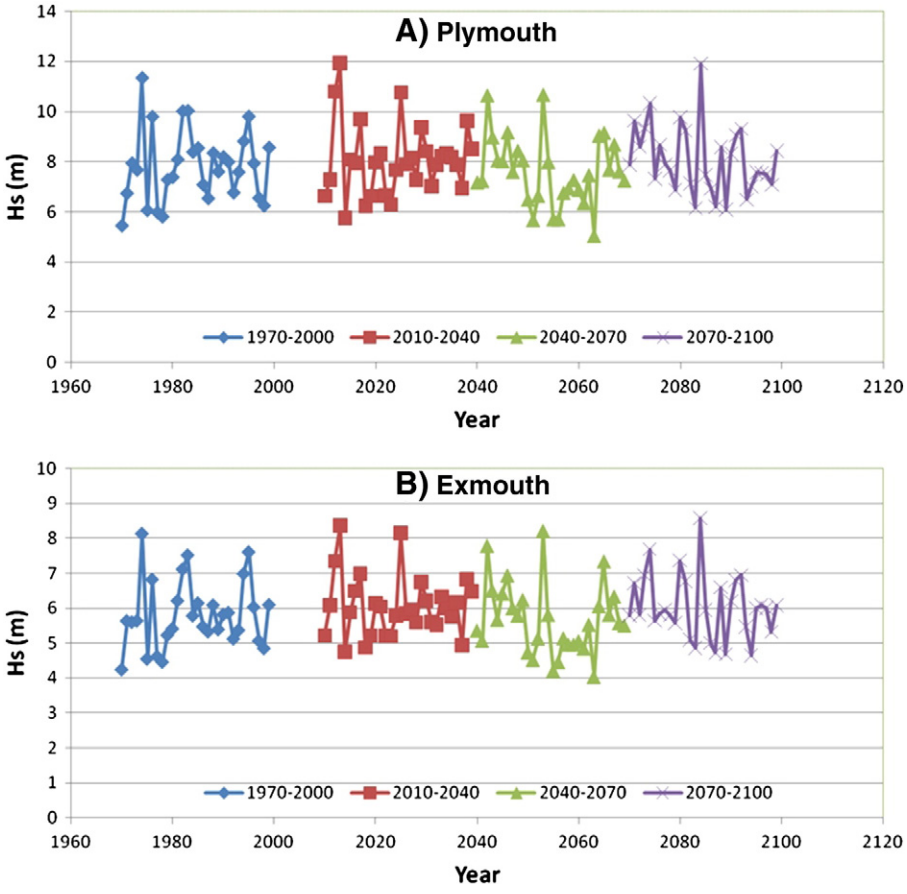

Fig. 24. Yearly mean water level at Plymouth (Devonport) and Weymouth.

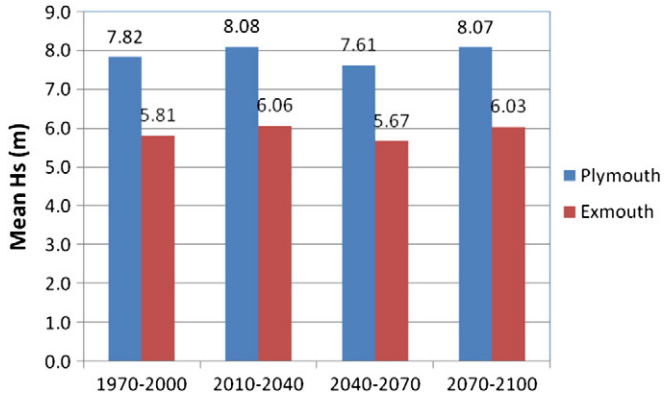

Fig. 25. Mean significant wave heights at Plymouth and Exmouth for three future time slices and present conditions.

wave heights for the periods of 2010–2040 and 2070–2100 are higher than that at present conditions, but the wave height during 2040–2070 is lower than the present wave height.

The joint wave and surge distributions for the 3 future scenarios are shown in Fig. 26, for Exmouth. The distribution shapes are very similar, indicating insignificant changes for the A1B greenhouse gas emission scenario.

Predicted extreme significant wave heights at Plymouth for time slices: 1970–2000 (present); 2010–2040 (short-term); 2040–2070 (mid-term); and 2070–2100 (long-term climate scenarios) are shown in Table 8.

Table 8
Predicted (Gumbel) extreme significant wave height (m) at Plymouth for 4 time slices.

Return period (years)	Present (1970–2000)	Short-term (2010–2040)	Mid-term (2040–2070)	Long-term (2070–2100)
5	9.085	9.358	8.827	9.277
20	10.936	11.232	10.615	11.046
50	12.111	12.422	11.750	12.169
100	12.991	13.314	12.601	13.011

5.4. Results

5.4.1. Flooding maps for future climate

The flooding predictions are focused on the Teign Estuary. The flooding maps for future scenarios considered the projected sea level rise recommended in the Planning Policy Statement 25 — PPS25 (DCLG, 2010). Table 9 shows the extreme sea level for different climate change scenarios combining the projected net sea level rise from the year 2010 to 2100 based on the PPS25.

The flooding maps obtained using the data in Table 9 were incorporated into a Geographic Information System software (ArcGIS®), combining information from LiDAR, topographical data obtained from the Plymouth Coastal Observatory (http://www.channelcoast.org) and from the DIGIMAP (EDINA, 2011). The flooding surface was generated using the toolboxes and a flood simulation model (Kwan, 2011).

Particular attention was paid to three areas within this study site: the Newton Abbot area in the upstream of the estuary, and two areas towards the downstream of the estuary — Shaldon and Teignmouth (see Fig. 27). Teignmouth is found to be subject to tidal flood risk for a return period as low as 20 years, under the present sea level rise scenario. However, the flooding situation is relatively mild in comparison to Shaldon and Ringmore. Although Teignmouth is a small port town, its importance lies in the fact that the main railway line runs through it. The simulation results identified that the railway line is subject to flood risk along the section running from the north of the Old Quay in Teignmouth to the west of Shaldon Bridge. Although the estimated flood depth is only around 0.5 m–1.0 m and would only happen in the long-term scenarios, the disruption of the rail services by the breach of the seawall will inevitably cause economic losses and inconvenience to the passengers.

Results for future scenarios show that flooding only occurs for a 1000 year return period high water level or greater, in the mid-term scenario. Fig. 27 clearly shows that flooding will occur first in Ringmore. For the long-term scenarios, flooding at Shaldon and Ringmore occurs for long-term scenarios with 1/200 and 1/1000 year return periods. Water levels in this area could be as high as 2 to 3 m, which will inevitably cause serious economic losses in the area.

5.4.2. Coastal erosion analysis for future climate

Due to the south-west main railway line between Exmouth and Teignmouth, which is well maintained, and other permanent coastal defence structures, such as seawalls and groynes, the coastline position has not been altered significantly for decades. However, it has been observed that beach profiles at the various locations have significant alternations under storm conditions.

Erosion and accretion in the Teignmouth area are expected to remain the same as for present conditions, in future scenarios. This is mostly due to the wave direction conditions considered in the climate scenarios (see Fig. 28), which are sustaining the same directions as in present conditions. That is to say that the areas that are eroding or accreting in the present conditions will show a similar behaviour in the future, as shown in the erosion/accretion maps produced (see Fig. 29). Results show that most of the Teign estuary is well protected by the coastal defences, mostly in the form of seawalls. However, the coastline in the south side of the estuary is subject to erosion under the future scenarios. The coastline north of the Teign Estuary and the sand spit of the Dawlish are also expected to suffer from erosion.

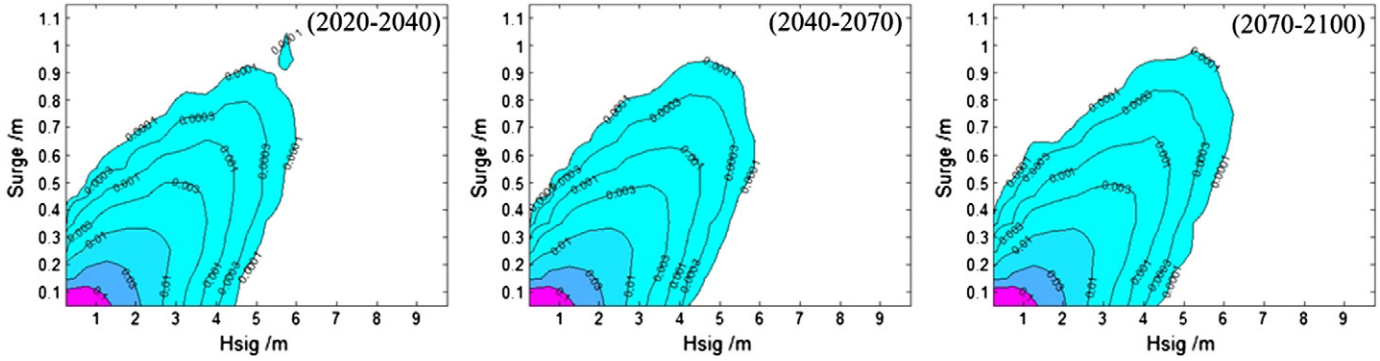

Fig. 26. Joint wave and surge distributions at Exmouth for future scenarios (contours in log scale).

Table 9
Extreme sea level (m AOD) for the future scenarios and different return periods in the Teign Estuary.

Return period (Years)	Climate scenarios for sea level rise and storm surge			
	Present (1970–2000)	Short-term (2010–2040)	Mid-term (2040–2070)	Long-term (2070–2100)
20	2.955	3.008	3.248	3.593
100	3.157	3.210	3.450	3.795

6. Discussion

The range of study of sites — Bellocchio, Varna, Santander and Plymouth, although characterised by low open beaches, offer a variety of characteristics in terms of the level of development and coastal protection existing in each area, as well as to the hydro/meteorological forcings acting on them. This, combined with the varying availability of data (bathymetry, topography, wave, tides, storm surge), allowed for the implementation of a series of models and analysis techniques that exemplify the proposed methodology for the estimation of flood and erosion hazards. This methodology consists of three main parts:

a) generation of the present and future climate scenarios;
b) hydrodynamic characterisation of the identified hazards;
c) flood and erosion hazard simulations/estimation.

Here we discuss the main advantages and disadvantages of each of these approaches and their application, based on results obtained at the 4 study sites analysed (see summary in Table 10).

The generation of present and future climate scenarios was performed in a very similar way for all case studies, i.e. statistical analysis of existing data bases (reanalysis data from local wave and storm surge models, and river discharge data), and the consideration of the IPCC A1B and B1 gas emission scenarios to adjust the sea states for expected future conditions. The main difference concerned the varying hydrometeorological forcing, including waves and surge, being an important source of flood hazard in Varna's case, while at sites such as Bellocchio and Plymouth tidal variations contribute significantly to wave and storm forcing, thus playing a more important role. The obtained sea states (present and future) correspond to offshore conditions and therefore, in all cases, wave transformation models had to be implemented to obtain the hydrodynamic conditions at the shore. The range of models used went from simplified equations such as those implemented in Bellocchio, to more sophisticated, widely used third-generation spectral wave models such as WAM (Komen et al., 1994) and Wavewatch III (Tolman, 1999) for deepwater, in combination with SWAN (Booij et al., 1999) for the nearshore transformation. There are many papers that discuss the advantages and disadvantages of these models (see Cavaleri, 2006 for a review), and the decision as to which one to use, was down to practical considerations. WAM is the predecessor of these three and although semi-proprietary versions now exist, no strong central support has been given since the 1990's; SWAN and Wavewatch III, on the other hand, are actively supported and freely available. All these models provide an excellent level of accuracy in wave forecasting, however, they seem to have intrinsic limitations that might only be overcome with the gradual introduction of new methods towards an eventual deterministic depiction of the sea surface (Cavaleri, 2006).

The most significant difference as to the approach employed at each case study corresponded to the estimation of the flood and erosion hazard and the definition of its pathways. These varied from the use of highly sophisticated 2D commercial hydrodynamic models, such as MIKE21, to simulate flood depths and velocities as a dam break at Bellocchio, to the estimation of the statistical distribution of the flood and erosion hazards at Santander for their categorization into

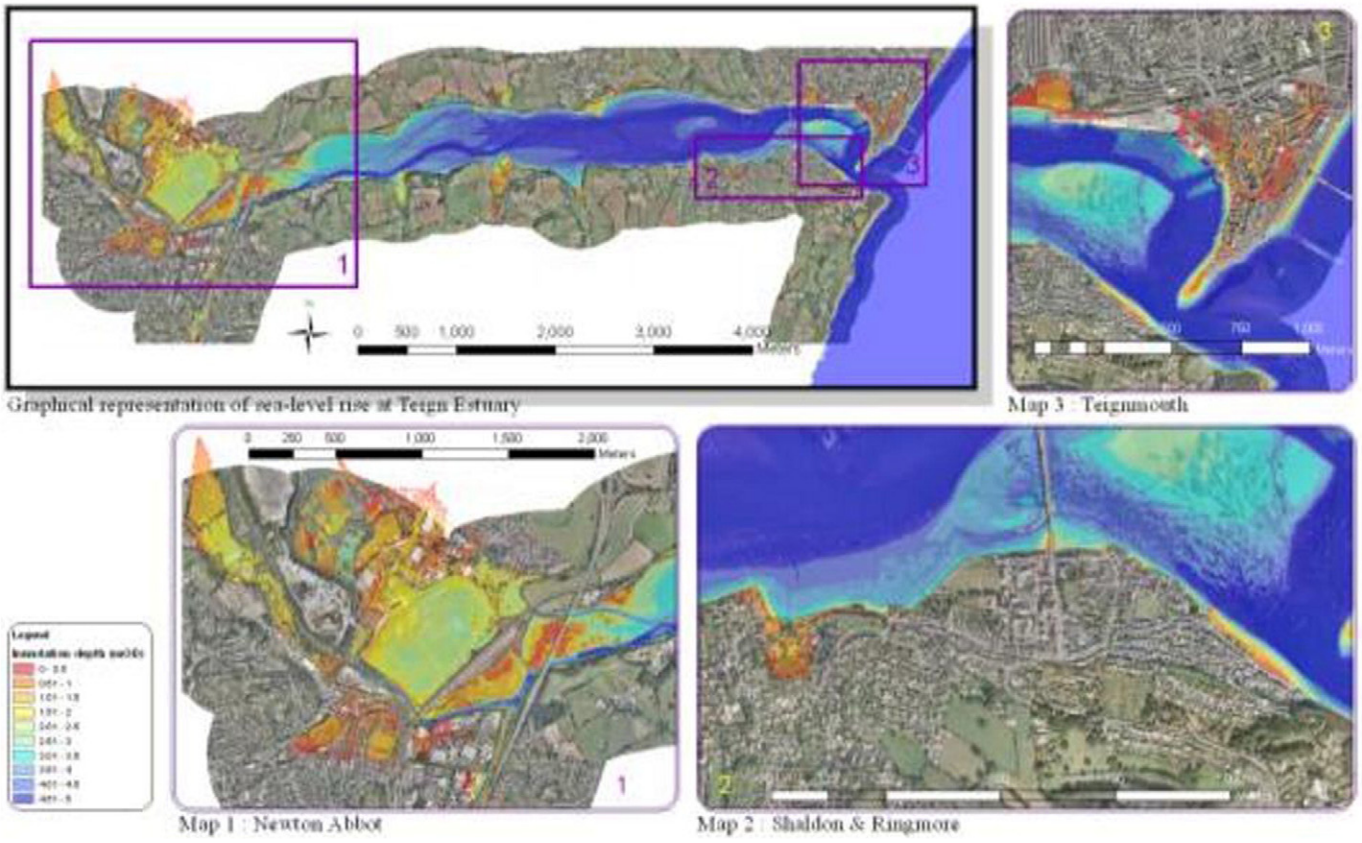

Fig. 27. Flood simulation for sea level rise scenario Mid-term scenario (1/1000 year).

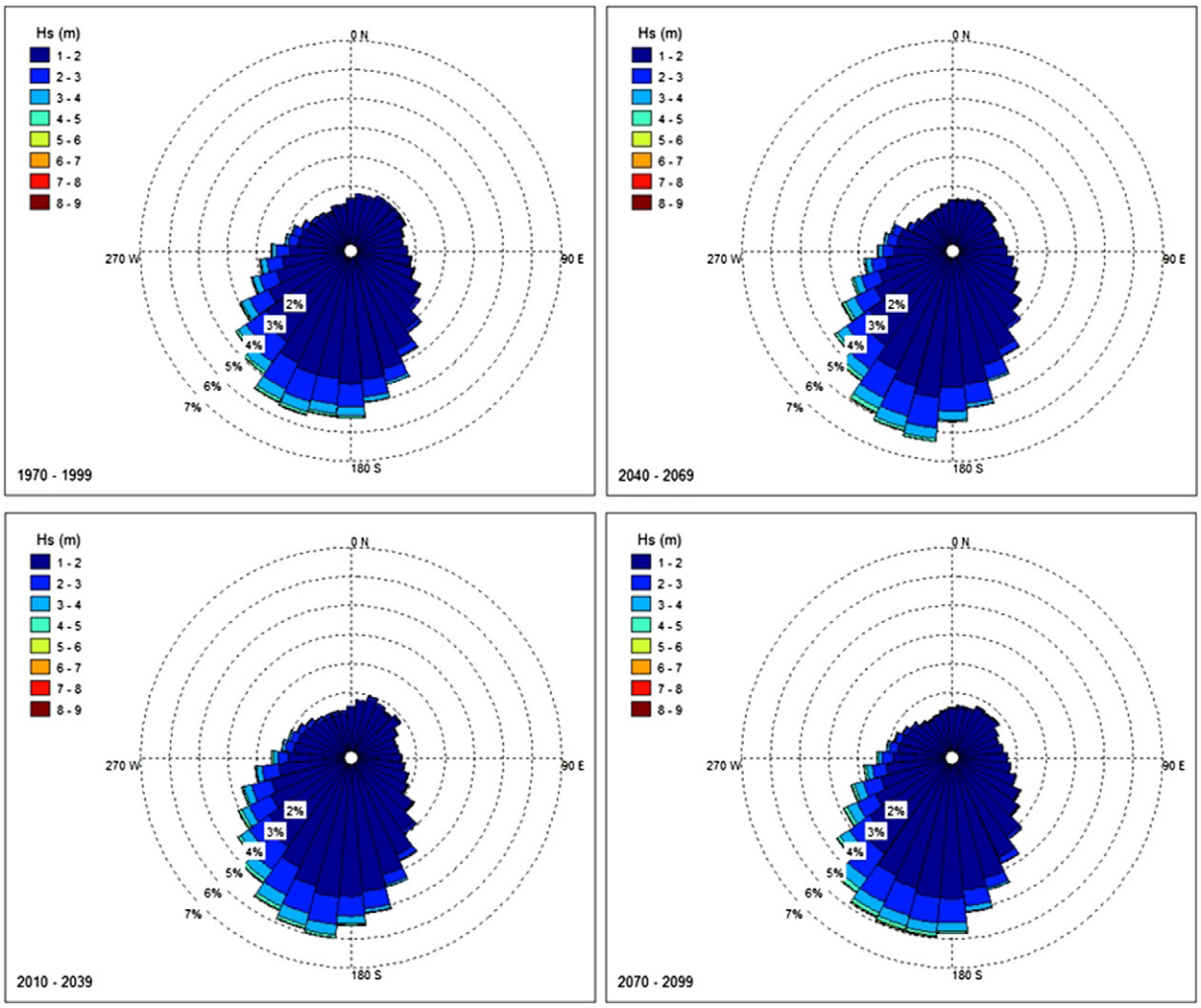

Fig. 28. Exmouth wave roses for the different climate scenarios (present, short-term, mid-term and long-term).

homogenous impact units. Additionally, the methodology implemented at Bellocchio or Plymouth, given that high resolution topography (LiDAR) was used in combination with a high resolution hydrodynamic model, allowed for a quantitative evaluation of the flood hazard, in comparison to the results obtained for Santander, for example, which are limited to a qualitative assessment. The difference, in terms of generating management strategies is that in the case of Bellocchio and Plymouth it is possible to assess the effectiveness of the existing defence structures and design a strategy accordingly, whereas in the case of Santander or Varna, results only allow us to compare hazard potential between different parts of the study site. Both approaches are, nevertheless, very useful and choosing one over the other must be done on the basis of what type of information needs to be produced, as well as the available time and computational resources. On one hand there are coastal models, such as MIKE21 (DHI, 2007), Delft3D (Lesser et al., 2004) and Telemac2D (Hervouet, 2000), which present their own set of challenges in terms of their ability to solve acting processes, such as wave breaking, wave current interaction, boundary effects and bottom friction. A qualitative assessment, in turn, has the advantage of being more efficient in terms of time and computing effort, and can therefore be used for short term hazard assessment when storm forecasts are available. Also, qualitative and simplified methods may allow the comparison of many different scenarios at limited costs, and be embedded in decision support tools (Zanuttigh et al., 2014–in this issue). This is of great value in enabling local populations and civil protection agencies to identify and act to minimise risks.

7. Conclusions

The application of a methodology to assess flooding and erosion risk in coastal areas is presented. The approach is focused on the first two steps of the Source–Pathway–Receptor–Consequences (SPRC) model and, among other things, allows:

- derivation of water levels/flood maps for events more extreme than have been recorded so far
- derivation of results for specific return periods
- prediction of the impacts of climate change
- assessment of the 'benefits' of different flood defence interventions
- prediction of what would happen if defences fail.

The characterisation of the sources of risk was undertaken through statistical analysis of measured and hindcast data, as well as hydrodynamic modelling of the identified sources (including waves, tides, winds, storm surge and river discharge). The description of the pathways of risk, on the other hand, was performed through flood and erosion modelling, using the modelled sources as input. From the analysis, it was determined that the risk of flooding and erosion at the four studied sites is significant at present and, although caused by different hazards, it is expected to increase in the future as a result of climate change and, where relevant, subsidence. It was also found that the greatest threat posed by future climate change will be the relative rise of sea level, as opposed to changes in storminess patterns. Existing natural and man-made sea defences were found to be crucial in the delimitation of the extent of flooding and erosion,

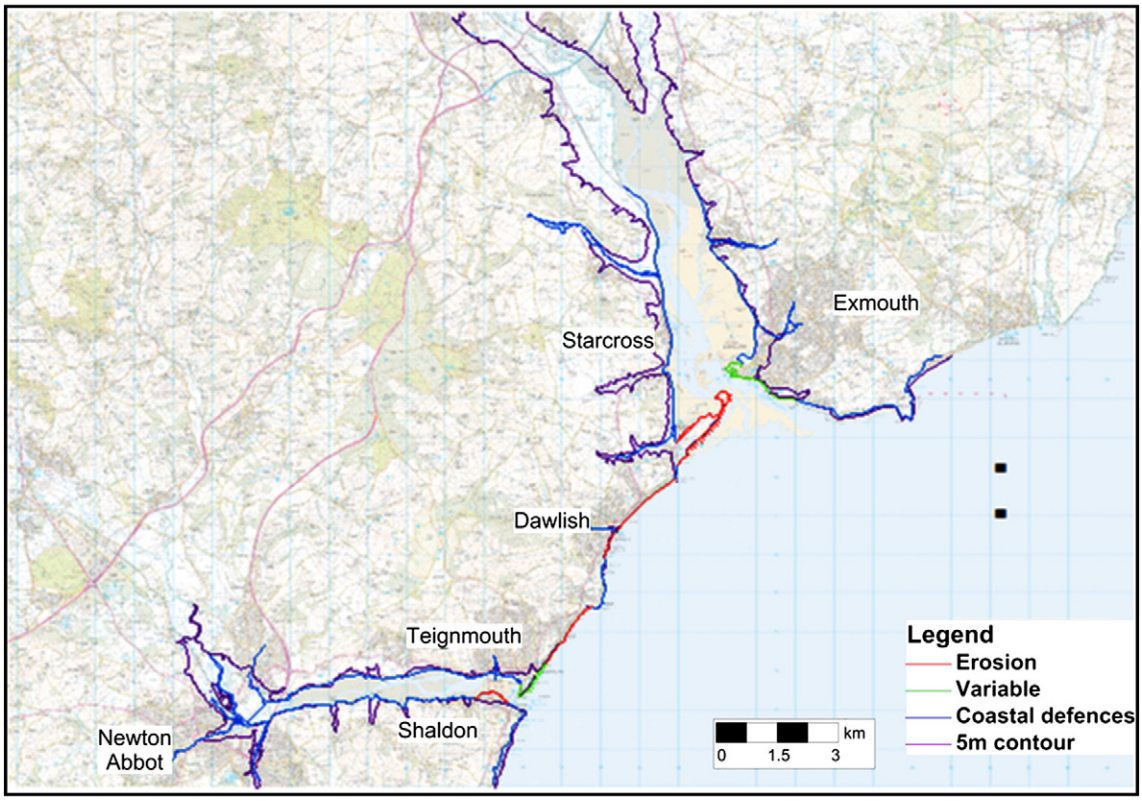

Fig. 29. Erosion and accretion maps for present and future conditions.

rendering their consideration as important as the nature and magnitude of the identified sources of risk.

Given the great variability in both the type of sources of risk identified and the morphological characteristics of the studied sites, the implemented approach was simplified through the categorisation of levels of risk for both sources and morphological features, into homogenous impact units. This highlights the applicability of the approach to a wide range of locations and scales, regardless of their characteristics. Furthermore, the use of models and techniques with varying degrees of complexity and detail, for the study of both the sources and the pathways, makes the proposed methodology one that can be adapted depending on the availability of data, as well as time and computing resources. This is particularly important, if this methodology is to be applied for management purposes in developing countries, or if it is intended to be used as a proxy for risk by the population and civil protection agencies, when warnings for particular hazards have been issued. On the other hand, it has been shown that when powerful models and high resolution topographical data are used the level of detail achieved by some flood and erosion predictions can provide a solid base for the development of specific risk management strategies, such as the design and maintenance of sea defences and other coastal protection schemes.

Table 10
Comparison of data bases and methodologies used in each case study.

Study site	Characteristics	Generation of forcing scenarios	Characterisation of the hazards (sources of risk)	Flood and erosion modelling (pathways of risk)
Bellocchio, Italy	Low open beaches	• Statistical analysis of SGA-CLM wave and storm surge data set • IPCC A1B scenario	• Matlab® code for offshore to nearshore wave transformation	• Failure mechanism • Flood modelling with MIKE21 (dam break approach) • Generation of detailed quantitative flood maps using LiDAR topography
Varna, Bulgaria	Low open beaches (tide-less)	• Atmospheric reanalysis data and CLM regional climate model • IPCC A1B and B1 scenarios	• Models WAM and SWAN for offshore and nearshore wave transformations • Model MATO for storm surge modelling • Prototype storms	• Erosion modelling with IO-BASMM, SBeach and XBeach (along typical profiles) • Flood modelling with IO-BASMM • Generation of qualitative flood and erosion maps
Santander, Spain	Spit, pocket beaches and embayed beaches	Statistical analysis of hindcast data from the GOW numerical data base	• Transformation of offshore sea states using models Wavewatch III and SWAN • Storm surge reanalysis data from model GOS	• Flood hazard estimation through FL = MSL + AT + η_s + $R_{u2\%}$ • Erosion hazard determination with Miller and Livermont (2008) approach • Statistical analysis of the hazard $fz(z)$ (GEV distribution)
Plymouth, UK	Open beaches (estuary influenced)	• Statistical analysis of wave and storm surge data from model POLCOHS/ProWAM • IPCC A1B scenario	• Process model for wave transformation with nearshore defences	• Flood simulation model (Kwan, 2011) • Generation of flood maps using LiDAR topography

Acknowledgments

The authors are very grateful to all researchers involved in the development of this paper and the results presented in it, in particular to Jose M. Horrillo-Carballo and Raul González, from University of Plymouth and Gerardo Durán, from UNAM for their technical support. Additional credit goes to Nikolay Valchev from IO-BAS; Panayotis Prinos, Yannis Krestenitis, Yannis Androulidakis and Katerina Kombiadou from AUTH; Ralf Weisse from HZG; and Alexander Polonsky from MHI for their contribution to the Varna study site. The support of the European Commission through FP7.2009-1, Contract 244104 - THESEUS ("Innovative technologies for safer European coasts in a changing climate"), is gratefully acknowledged.

References

Abascal, A.J., Castanedo, S., Medina, R., 2010. GOS, un reanálisis de marea meteorológica de 60 años de alta resolución para el sur de Europa. I Encuentro Oceanografía Física Española. (In Spanish).

Andreeva, N., Valchev, N., Trifonova, E., Eftimova, P., Kirilova, D., Georgieva, M., 2011. Literary review of historical storm events in the western Black Sea. Proc. of Union of Scientists-Varna, Marine Sciences 105–112.

Belberov, Z., Zahariev, V., Krylov, Y., Kostichkova, D., Manyarova, R., Polyakov, Y., 1982. Analysis of the catastrophic storm in February 1979 near the Bulgarian Black sea coast. Oceanology 9, 3–12 (Sofia, In Bulgarian).

Booij, N., Ris, R.C., Holthuijsen, L.H., 1999. A third-generation wave model for coastal regions, Part 1: model description and validation. J. Geophys. Res. 104, 7649–7666.

Camus, P., Méndez, F.J., Medina, R., Cofiño, A.S., 2011. Analysis of clustering and selection algorithms for the study of multivariate wave climate. Coast. Eng 58 (6), 453–462.

Cavaleri, L., 2006. Wave modelling—where to go in the future. Bull. Am. Meteorol. Soc. 207–214.

Chen, Y., Pan, S., Hewston, R., Cluckie, I., 2010. Ensemble modelling of tides, surge and waves. Proceedings of the 20th International Offshore (Ocean) and Polar Engineering Conference, CD-ROM.

Coles, S.G., 2001. An Introduction to Statistical Modeling of Extreme Values. Springer, London (208 pp.).

Department for Communities and Local Government—DCLG, 2010. Planning Policy Statement 25: Development and Flood Risk. [Online]. Available at: http://www.communities.gov.uk/documents/planningandbuilding/pdf/planningpolicystatement25.pdf.

DHI, 2007. MIKE 21 & MIKE 3 Flow Model FM—Sand Transport Module. Rep. Horsholm, Denmark (10 pp.).

EDINA, 2011. DIGIMAP Collection. http://edina.ac.uk/digimap/ [accessed: February, 2011].

EUROSTAT, 2009. Statistics in focus. http://ec.europa.eu/eurostat.

Galiatsatou, P., Prinos, P., Valchev, N., Trifonova, E., 2012. Analysis of extreme marine events causing flooding in Varna region. Turk. J. Fish. Aquat. Sci. (ISSN: 1303-2712) 12, 523–531. http://dx.doi.org/10.4194/1303-2712-v12_2_44.

Hemer, M.A., Church, J.A., Hunter, J.R., 2010. Variability and trends in the directional wave climate of the Southern Hemisphere. Int. J. Climatol. 30, 475–491.

Hervouet, J.M., 2000. The TELEMAC modelling system. Hydrol. Process. SI 14 (13), 2209–2210.

Holt, J.T., James, D.T., 2001. An s-coordinate density evolving model of the northwest European continental shelf: 1, Model description and density structure. J. Geophys. Res. 106, 14,015–14,034.

Horrillo-Carballo, J.M., Pan, S., Reeve, D.E., Simmonds, D.J., Greaves, D., Fox, A., 2012. Modelling extreme wave events (present and future scenarios) in Southwest England. Proceedings of ICCE 2012, Santander (8 pp.).

IPCC, 2007. Climate change 2007: synthesis report. (Core Writing Team) In: Pachauri, R.K., Reisinger, A. (Eds.), Contribution of Working Groups I, II and III to the Fourth Assessment Report of the Intergovernmental Panel on Climate Change. IPCC, Geneva, Switzerland (104 pp.).

JNCC, 1997. The Habitats Directive: Selection of Special Areas of Conservation in the UK. Report NO. 270. Defra.

Kalnay, E., Kanamitsu, M., Kistler, R., Collins, W., Deaven, D., Gandin, L., Iredell, M., Saha, S., White, G., Woollen, J., Zhu, Y., Chelliah, M., Ebisuzaki, W., Higgins, W., Janowiak, J., Mo, K.C., Ropelewski, C., Wang, J., Leetmaa, A., Reynolds, R., Jenne, R., Joseph, D., 1996. The NCEP/NCAR 40-year reanalysis project. Bull. Am. Meteorol. Soc. 77 (3), 437–471.

Kohonen, T., 2000. Self-Organizing Maps, 3rd ed. Springer-Verlag, Berlin.

Komen, G.J., Cavaleri, L., Donelan, M., Hasselmann, K., Hasselmann, S., Janssen, P.A.E.M., 1994. Dynamics and Modelling of Ocean Waves. Cambridge University Press (532 pp.).

Krestenitis, Y.N., Androulidakis, Y.S., Kontos, Y.N., Georgakopoulos, G., 2010. Coastal inundation in the north-eastern Mediterranean coastal zone due to storm surge events. J. Coast. Conserv. 14, 1–16. http://dx.doi.org/10.1007/s11852-010-0090-7.

Kwan, S.H., 2011. GIS Modelling of Flood on the South Devon Coast. (MSc. Thesis) Plymouth University (September 2011).

Larson, M., Kraus, N.C., 1989. Prediction of beach fill response to varying waves and water level. Proceedings of Coastal Zone'89, American Society of Civil Engineers, pp. 607–621.

Lesser, G.R., Roelvink, J.A., van Kester, J.A.T.M., Stelling, G.S., 2004. Development and validation of a three-dimensional morphological model. Coast. Eng. 51, 883–915.

Li, Y., Simmonds, D.J., Reeve, D.E., 2008. Quantifying uncertainty in extreme values of design parameters with resampling techniques. Ocean Eng. 35 (10), 1029–1038.

Martinelli, L., Zanuttigh, B., Corbau, C., 2010. Assessment of coastal flooding hazard along the Emilia Romagna Littoral, IT. Coast. Eng. 57 (11–12), 1042–1158.

Méndez, F.J., Menéndez, M., Luceño, A., Losada, I.J., 2006. Estimation of the long-term variability of extreme significant wave height using a time-dependent POT model. J. Geophys. Res. 111, C07024.

Miller, J.K., Livermont, E., 2008. An index for predicting storm erosion due to increased waves and water levels. Solutions to Coastal Disaster Congress 2008.

Mínguez, R., Espejo, A., Tomás, A., Méndez, F.J., Losada, I.J., 2011. Directional calibration of wave reanalysis databases using instrumental data. J. Atmos. Ocean. Technol. 28, 1466–1485.

Narayan, S., Nicholls, R.J., Clarke, D., Hanson, S., Reeve, D., Horrillo-Carballo, J., le Cozannet, G., Hissel, F., Kowalska, B., Parda, R., Willems, P., Ohle, N., Zanuttigh, B., Losada, I., Ge, J., Trifonova, E., Penning-Roswell, E., Vanderlinden, J.P., 2013. Evaluating the 2D Source–Pathway–Receptor model for flood risk assessment. Coast. Eng. http://dx.doi.org/10.1016/j.coastaleng.2013.10.021 (in this issue).

Nicholls, R.J., Wong, P.P., Burkett, V.R., Codignotto, J.O., Hay, J.E., McLean, R.F., Ragoonaden, S., Woodroffe, C.D., 2007. Coastal systems and low-lying areas. Climate change 2007: impacts, adaptation and vulnerability. In: Parry, M.L., Canziani, O.F., Palutikof, J.P., van der Linden, P.J., Hanson, C.E. (Eds.), Contribution of Working Group II to the Fourth Assessment Report of the Intergovernmental Panel on Climate Change. Cambridge University Press, Cambridge, UK, pp. 315–356.

Nielsen, P., Hanslow, D.J., 1991. Wave run-up distributions on natural beaches. J. Coast. Res. 7 (4), 1139–1152.

Pan, S., Chen, Y., Wolf, J., Du, Y., 2009. Modelling of waves in the Irish Sea: effects of oceanic wave and wind forcing. Ocean Dyn. 59 (6), 827–836.

Pickands, J., 1975. Statistical inference using extreme order statistics. Ann. Stat. 3, 119–131.

Posada, G., Simmonds, D., Silva, R., Pedrozo, A., 2008. A 2D hydrodynamic model with multi-quadtree mesh. In: Alan, I. (Ed.), Ocean Engineering Research Advances. Nova Publishers, Prescot, pp. 205–241 (Chapter 8, ISBN 978-1-60021-777-7,1-60021-777-X).

Preti, M., De Nigris, N., Morelli, M., Monti, M., Bonsignore, F., Aguzzi, M., 2009. State of the Emilia-Romagna Littoral at 2007 and Ten-Years Management Plan, I quaderni dell'ARPA. Bologna In Italian, abstract in English.

Reeve, D.E., 1996. Estimation of extreme Indian monsoon rainfall. Int. J. Climatol. 16 (1), 105–112.

Reguero, B.G., Menéndez, M., Méndez, F.J., Mínguez, R., Losada, I.J., 2012. A Global Ocean Wave (GOW) calibrated reanalysis from 1948 onwards. Coast. Eng. 65, 38–55.

Roelvink, D., Reniers, A., Van Dongeren, A., Thiel, Van, de Vries, J., McCall, R., Lescinski, J., 2009. Modelling storm impact on beaches, dunes and barrier islands. Coast. Eng. 56, 1133–1152.

Stakev, M., 1980. About the break-down state of some coastal structures after the storm in February 1979. Shipbuilding Navigation 10, 26–30 (in Bulgarian).

Stockdon, H.F., Holman, R.A., Howd, P.A., Sallenger Jr, A.H., 2006. Empirical parameterization of setup, swash, and runup. Coast. Eng. 53 (7), 573–588.

Thorne, C., Evans, E., Penning-Rowsell, E., 2007. Future Flooding and Coastal Erosion Risks. Thomas Telford, London.

Tolman, H.H., 1999. User manual and system documentation of WAVEWATCH-III version 1.18. NOAA/NWS/NCEP/OMB Technical Note 166. (110 pp.).

Trifonova, E.V., 2007. Modelling of cross shore profile changes under combination of extreme storm events. Proceedings of the 4th International Conference "Port Development and Coastal Environment - PDCE" (Varna, Bulgaria), pp. 301–311.

Trifonova, E., Demireva, D., 2003. An investigation of sea level fluctuations in Varna and Bourgas. Proc. Inst. Oceanol. 4, 3–9.

Trifonova, E., Valchev, N., Andreeva, N., Eftimova, P., 2010. Reconstruction of severe storms in the Western Black Sea and assessment of their impact on the coast. Proc 10th Int. Conf. on "Marine Sciences and technologies—Black Sea'2010", Varna, Bulgaria, pp. 254–260.

Trifonova, E., Valchev, N., Andreeva, N., Eftimova, P., 2011. Critical storm thresholds for morphological changes in the western Black Sea coastal zone. Geomorphology 143–144 (March 2012), 81–94. http://dx.doi.org/10.1016/j.geomorph.2011.07.036.

Umgiesser, G., Martinelli, L., Zanuttigh, B., Bellafiore, D., Ferrarin, C., 2011. Sea level rise and coastal flood protection in Cesenatico, Italy. Proc. Acqua Alta 2011 (Exhibition and Int. Conf. On climate impact, flood protection and hydraulic engineering), Hamburg, 11–13 October 2011.

Uppala, S.M., Kallberg, P.W., Simmons, A.J., Andrae, U., Bechtold, V.D., Fiorino, M., Gibson, J.K., Haseler, J., Hernandez, A., Kelly, G.A., Li, X., Onogi, K., Saarinen, S., Sokka, N., Allan, R.P., Andersson, E., Arpe, K., Balmaseda, M.A., Beljaars, A.C.M., Van De Berg, L., Bidlot, J., Bormann, N., Caires, S., Chevallier, F., Dethof, A., Dragosavac, M., Fisher, M., Fuentes, M., Hagemann, S., Holm, E., Hoskins, B.J., Isaksen, L., Janssen, P.A.E.M., Jenne, R., McNally, A.P., Mahfouf, J.F., Morcrette, J.J., Rayner, N.A., Saunders, R.W., Simon, P., Sterl, A., Trenberth, K.E., Untch, A., Vasiljevic, D., Viterbo, P., Woollen, J., 2005. The ERA-40 re-analysis. Q. J. R. Meteorol. Soc. 131, 2961–3012.

Valchev, N., Trifonova, E., 2009. Wave climate clustering to define threshold values with respect to the expected morphological response. J. Coast. Res. SI 56, 1666–1670 ((Proceedings of the 10th International Coastal Symposium), Lisbon, Portugal).

Valchev, N., Davidan, I., Belberov, Z., Palazov, A., 2007. Practicability of wind waves simulations based on the global reanalysis wind fields in the Black Sea deep and shallow waters. 4th Int. Conf. "Port Development and Coastal Environment—2007", Varna, Bulgaria, pp. 185–191.

Valchev, N., Trifonova, E., Andreeva, N., 2012. Past and recent trends in the western Black Sea storminess. Nat. Hazards Earth Syst. Sci. 12, 961–977. http://dx.doi.org/10.5194/nhess-12-961-2012.

van der Meer, J.W., Briganti, R., Zanuttigh, B., Wang, B., 2005. Wave transmission and reflection at low-crested structures: design formulae, oblique wave attack and spectral change. Coast. Eng. 52 (10), 915–929.
WDCC, 2009. http://cera-www.dkrz.de/World (Data Centre for Climate, CERA-DB).
Weisse, R., Bellafiore, D., Menéndez, M., Méndez, F., Nicholls, R.J., Umgiesser, G., Willems, P., 2014. Changing extreme sea levels along European coasts. Coast. Eng. 87, 4–14 (in this issue).
Woolf, D.K., Challenor, P.G., Cotton, P.D., 2002. Variability and predictability of the North Atlantic wave climate. J. Geophys. Res. 107 (C10), 3145.
Zanuttigh, B., 2011. Coastal flood protection: what perspective in a changing climate? The THESEUS approach. Environ. Sci. Pol. http://dx.doi.org/10.1016/j.envsci.2011.03.015.
Zanuttigh, B., Zagonari, F., Bagli, S., Pescaroli, G., Bozzeda, F., Hoggart, S., Nicholls, R.J., Garcia-Alonso, E., Losada, I.J., Vanderlinden, J.P., 2014. THESEUS decision support system for coastal risk management. Coast. Eng. 87, 218–239 (in this issue).